Extending the Balbi fire spread Model for field scale conditions: the case of shrubland fires

François Joseph Chatelon, Jacques Henri Balbi, Miguel Cruz, Dominique Morvan, Jean Louis Rossi, Carmen Awad, Nicolas Frangieh, Jacky Fayad, Thierry Marcelli

Extending the Balbi fire spread Model for field scale conditions: the case of shrubland fires

François Joseph CHATELON[1], Jacques Henri BALBI[1], Miguel G. CRUZ[2], Dominique MORVAN[3], Jean Louis ROSSI[1] , Carmen AWAD[1], Nicolas FRANGIEH[1], Jacky FAYAD[1] and Thierry MARCELLI[1,*]

[1] Université de Corse, Systèmes Pour l'Environnement UMR-CNRS 6134, Campus Grimaldi, BP 52 20250 Corte, France.

[2] CSIRO, GPO Box 1700, Canberra, ACT 2601, Australia.

[3] Aix Marseille Univ, CNRS, Centrale Marseille, M2P2, Marseille, France.

Abstract: The 'Balbi model' is a simplified rate of fire spread model aimed at providing fast and accurate simulations for fire spread that can be used by fire managers under operational conditions. This model describes the steady-state spread rate of surface fires by accounting for both radiation and convection heat transfer processes. In the present work the original Balbi model developed for laboratory conditions is improved with changes that address specificities of outdoor fires, such as fuel complexes with a mix of live and dead materials, a larger scale and an open environment. The model is calibrated against a small training dataset (n=25) of shrubland fires conducted in Turkey. A sensitivity analysis of model output is presented and its predictive capacity against a larger independent dataset of experimental fires in shrubland fuels

[*] Corresponding Author. Email: marcelli_t@univ-corse.fr

from different regions of the world (Europe, Australia, New-Zealand and South Africa) is tested. A comparison with older versions of the model and a generic-empirical model is also conducted to investigate contrasts with other models and quantify improvements in the predictive capacity of the model. The improved model remains physics-based, faster than real time and fully predictive.

Keywords: Fire spread, shrubs, live fuel, radiation, convection, fire dynamics, model performance, physical model, steady-state model

Introduction

Many regions of the world are severely hit by severe wildfires. As the result of interactions between climate, fuels, topography and people, wildfires can have negative socioeconomic and ecological consequences (Finlay *et al.* 2012; Meyer *et al.* 2013; Youssouf *et al.* 2014; Castro Rego *et al.* 2018; Dupuy *et al.* 2020; European Science & Technology Advisory Group 2020). They represent a significant factor changing ecosystem function and resilience (Wotton *et al.* 2003; Running 2006; Sağlam *et al.* 2008; Fernandes 2013; San-Miguel-Ayanz *et al.* 2013; Tang *et al.* 2015) and they pose a threat to human life, infrastructure and activites, particularly when fires spread into the Wildland-Urban Interface (Radeloff *et al.* 2005; Hammer *et al.* 2007; Keane *et al.* 2010). These negative impacts of wildfires have been exacerbated as a result of climate change (European Science & Technology Advisory Group 2020). The need for fire spread simulation tools (e.g. Finney (1998); Filippi *et al.* (2011); Mandel *et al.* (2011)) that aid emergency response, firefighting and fire management decision making has become more and more crucial. Development of new fire spread models that overcome previous ones constrains and limitations is one the the main aims of fire behaviour scientists around the globe.

Over the last three decades, significant advances made on physical and chemical modelling of wildland fire processes has contributed to the development of a significant number of models describing wildfire propagation. This model evolution reviewed by several authors (Weber 1991; Perry 1998; Pastor *et al.* 2003; Sullivan 2009a; b; c) is basically categorized in three main approaches: (1) mathematical or empirical models, (2) semi-empirical models and (3) physical models.

Statistical or empirical models (McArthur 1966; Noble *et al.* 1980; Cheney *et al.* 1998; Anderson *et al.* 2015; Rossa and Fernandes 2018) are generally built over a large set of observational data and they do not describe any physical mechanisms for heat transfer. The fire rate of spread is usually defined as a function of several independent variables such as wind

velocity, terrain slope angle, fuel moisture content and fuel structure variables (Cheney *et al.* 1998; Fernandes 2001; Keane 2019a). Semi-empirical models, such as the well-known Rothermel model (Rothermel 1972), are able to simplify the physical description of the fire spread processes while incorporating some key principles. Both the empirical and semi-empirical approach produced models that are applicable to operational conditions. For example, the Rothermel (1972) is at the core of fire behaviour prediction systems like BEHAVE (Andrews 1986) and FARSITE (Finney 1998). It is also incorporated in more comprehensive fire - weather prediction systems like WRF-SFIRE (Mandel *et al.* 2011; Kochanski *et al.* 2013).

In contrast, physical models are based on the understanding of physical and chemical processes determining wildland fire behaviour. These models describe how the heat, mass and momentum fluxes are transferred from the fuel burning zone or from the flame body to the unburnt fuel (Lattimer 2019). Detailed physical models based on multiphase modelling (Grishin 1997; Morvan *et al.* 2000) solve a system of partial differential equations strongly coupled obtained from the gaseous phase and the different solid phases and represent the physical basis of computational fluid dynamics (CFD) simulators such as FireStar2D (Morvan *et al.* 2009), FireStar3D (Frangieh *et al.* 2018; Morvan *et al.* 2018), FIRETEC (Linn and Cunningham 2005) or Wildland Urban Interface Fire Dynamics Simulator, WFDS (Mell *et al.* 2007). These CFD-models are of great interest to extend our understanding of the physics of the fire dynamics but they are not suitable for simulating fire spread at large scales and under time contraints because of the high computational requirements.

Simplified physical models (Pagni and Peterson 1973; Albini 1985, 1986; Koo *et al.* 2005; Balbi *et al.* 2007) are a family of models that can bridge the gap between the simple empirical models and complex physical models. They incorporate the most important physical processes without having the computational needs of a full physical model, allowing for their use in operational settings. These models require parameterization of certain intermediate processes,

but this parameterization can be done with only a few fires in contrast with the data needs for the development of empirical models. This is significant due to the costs and inherent limitations of conducting large scale, high intensity experimental fire programs.

The 'Balbi model' (Balbi *et al.* 2020) follows this concept. The model is a fully predictive simplified physical model for surface fire spread which takes into account meteorological (wind velocity), topographical (terrain slope angle) and fuel (fuel moisture and fuel bed structure) conditions. The model has been developed and parameterized to describe fire propagation in free spreading fires at a laboratory scale (e.g. Nelson Jr. and Adkins (1986); Catchpole *et al.* (1998)).

The main goal of this paper is to extend the previous work by introducing changes that allow its use in outdoor fires, where scale and fuel characteristics depart from the original model fitting. The parameterization is applied to shrubland fuel types, an interesting challenge for the proposed model due to the stratified fuel complex arrangement composed of vertically separated fuel layers (Cruz *et al.* 2013). The new formulation is evaluated through the analysis of the effect of environmental variables in the model ouput and against a large set of outdoor shrubland fires given in (Anderson *et al.* 2015). A comparison between the obtained model fit statistics with results from other models is also made.

Methods

Model idealization

The Balbi et al. (2020) model

The global structure of the model proposed by Balbi *et al.* (2020) is kept, with changes introduced that aim at simulate relevant processes occurring in shrubland fires. Following Chatelon *et al.* (2017) and Balbi *et al.* (2020), it is still assumed that the fresh airstream which

105 enters the flame base (the pyrolysis area) is divided in two layers (Fig. 1): the hot gases from
106 the upper layer are driven to the top of the flame base, due to buoyancy and create the free
107 flame structure above the vegetal stratum. The mixed air-pyrolysis gases from the lower layer
108 go out through the front panel of the fuel burning particles area and create an internal, or
109 combustion zone, flame which directly contacts the unburnt fuel.

110 The four energy contributions suggested by Balbi *et al.* (2020) are considered: (1) flame base
111 radiation (the fuel burning particles radiate towards the unburnt fuel); (2) flame radiation (the
112 flame body acts as a grey radiant panel); (3) convective cooling (the flame body creates a
113 indraught of fresh air coming from the unburnt zone which offsets the flame radiation and the
114 periodic free flame contact with unburnt fuels because of turbulent effects); and (4) convective
115 heating (hot gases flow from the combustion zone and impinge the unburnt fuel particles by
116 direct contact). Note that the convective cooling effect did not explicitly appear in the equation
117 of the model but is incorporated in the flame radiation modelling (Balbi *et al.* 2010).

118 The rate of spread was obtained using a simplified preheating balance and based on the fuel
119 load σ and fuel moisture content *m* of the dead fuel. The main equation of the model, in a
120 condensed form, is the following:

121 $$R = R_b + R_c + R_r \quad (1)$$

122 With

123 $$R_b = a_b \frac{\phi_b}{\sigma\, q} \quad (2)$$

124 $$R_c = a_c \frac{\phi_c}{\sigma\, q} \quad (3)$$

125 $$R_r = a_r \frac{\phi_r}{\sigma\, q} \quad (4)$$

where $R_\bullet$, $\phi_\bullet$, $a_\bullet$, are the contributions of heat transfer mechanisms to the ROS, heat fluxes and scaling factors, respectively. The term q represents the energy required for ignition:

$$q = C_p(T_i - T_a) + m\,(\Delta h + C_{pw}(T_{vap} - T_a)) \quad (5)$$

where C_p, C_{pw}, T_i, T_a, T_{vap}, Δh, m are specific heat of fuel and water, ignition, ambient and vaporization temperature, heat of latent evaporation and fuel moisture content respectively (see Table 1).

Changes in the scaling factors

The scaling factors in Eqns 2-4 are modified in order to take into account the live fuel. As the flame base scaling factor a_b increases with the fuel height and decreases with the extinction depth δ, it was defined in (Balbi *et al.* 2020) by the following relationship:

$$a_b = \min\left(2\frac{h}{\delta}, 1\right) \quad (6)$$

Two slight changes are made on Eqn 6. First, the factor 2 in Eqn 6 is removed because it is assumed that at field scale the soil absorbs a part of the flame base radiative flux unlike the laboratory experiments in which the ground reflects the flame base radiation. Second, following the work of De Mestre *et al.* (1989) about optical depth, Balbi *et al.* (2020) have defined the extinction depth as inversely proportional to the fuel porosity ($\delta = 2\pi/(s\,\beta_t)$), where s is the surface area to volume ratio and β_t is the total packing ratio (dead and live fuel load). So, considering the total leaf area S_t (equal to the double of total LAI (Keane 2019b)), the scaling factor a_b is changed in:

$$a_b = \min\left(\frac{S_t}{2\pi}, 1\right) \quad (7)$$

Moreover, as one part of the heat release affects the live fuel and assuming that the spread of the ignition interface mainly depends on the catalytic effect of dead fuel, the leaf areas ratio (dead and total) is added to the scaling factor a_b:

$$a_b = \min\left(\frac{S_t}{2\pi}, 1\right)\left(\frac{S}{S_t}\right)^2 \quad (8)$$

The square on the ratio S/S_t expresses the action of this 'energy sink' effect on both emitted and absorbed flame base radiation, where S is the leaf area (2 × LAI). As noticed by Chandler *et al.* (1983), it seems that live fuel properties have a role on fire behaviour but this role is not clear (Pimont *et al.* 2019) and still discussed in the literature. Inhere, it is assumed that the live fuel is not directly involved in movement of the ignition interface, but as it contributes a proportion of the heat released, the part of the heat which does not impinge the dead fuel material is added in the improved model as the ratio between dead leaf area and total leaf area (which is related to a ratio between dead and total packing ratio).

The scaling factor a_r related to the flame radiation heat flux is similarly modified but only the absorption of this heat flux by the unburnt fuel is concerned:

$$a_r = \min\left(\frac{h}{\delta}, 1\right)\frac{S}{S_t} = \min\left(\frac{S_t}{2\pi}, 1\right)\frac{S}{S_t} = \min\left(\frac{S}{2\pi}, \frac{S}{S_t}\right) \quad (9)$$

The scaling factor a_c related to the convective heat flux is significantly changed. It is now split up in three contributions which corresponds to energy losses:

$$a_c = a_{up}\, a_{lat}\, a_{liv} \quad (10)$$

The factor a_{liv} represents the heat provided to the unburnt live fuel and the same modelling as in the scaling factors a_b and a_r is chosen:

$$a_{liv} = \frac{S}{S_t} \quad (11)$$

The factor a_{lat} describes the heat loss on the lateral edges of the fire front. Balbi *et al.* (2020) assumed this factor was equal to 1 for a laboratory set up where lateral walls constrained lateral heat losses at the combustion zone level (Catchpole *et al.* 1998). In our present formulation it is assumed that this factor explicitly depends on the effective fireline width W_0 (Cheney and Gould 1995) but remains equal to 1 when W_0 is greater than 50 m. For the current analysis W_0 is represented by the ignition line length in (Anderson *et al.* 2015). W_0 in the dataset change with experimental source/fuel type. See appendix B for further discussion):

$$a_{lat} = \min\left(\frac{W_0}{50}, 1\right) \tag{12}$$

Finally the factor a_{up} expresses two combined effects. The first one corrects the amount of pyrolysis gases produced by the airstream below the streamline which enters the flame base at point E (see Fig. 1). Indeed, this zone delimited by points BB_0A_0E was approximated by the surface of the triangle BB_0F. The second effect corresponds to the heat remaining in the fuel burning particles area when the heat released to the upper part of the fuel is removed. This effect is assumed to be proportional to the total leaf area S_t ($S_t = s\ h\ \beta_t$, where h is the fuel bed depth and β_t the total packing ratio) and inversely proportional to the flux of gases moving upward i.e the upward gas velocity in the preheating zone which is proportional to the root square of the fuel bed depth (due to buoyancy forces). The parameter a_{up} is modelled according to the following empirical relationship:

$$a_{up} = a_M s\ \beta_t \sqrt{h} \tag{13}$$

With a_M being an empirically parameter fitted to a training dataset through a calibration protocol. After this fitting, a_M is considered a constant for the application of the model to simulating fire spread in shrubland fuel complexes.

Finally, combining Eqns 11-13, Eqn 10 yields:

$$a_c = a_M s\, \beta_t \sqrt{h} \min\left(\frac{W_0}{50}, 1\right) \frac{S}{S_t} \quad (14)$$

Changes in the convective heat contribution

According to (Balbi *et al.* 2020) the convective heat flux is modelled as:

$$\phi_c = \frac{\Delta H}{2\tau_0} \sigma s \min(h, \delta) \tan \gamma_c \quad (15)$$

Where ΔH and τ_0 are the heat of combustion of pyrolysis gases and the flame residence time parameter, respectively. The angle γ_c is defined as in Fig. 1 by:

$$\tan \gamma_c = \tan \alpha + \frac{U(L)}{u_c} \quad (16)$$

where $U(L)$, u_c and α are horizontal wind speed at point *B,* upward gas velocity at the top of the flame base and terrain slope angle, respectively.

Due to the vertical dimension of the fuel bed, namely due to the existence of live fuels on its top, the definition of $U(L)$ is slightly changed. It is expressed as a function of wind velocity U at flame mid-height and drag forces:

$$U(L) = U \frac{h}{h + \frac{H}{2}} exp(-K^* L) \quad (17)$$

where H, L and K^* are the flame height, flame depth and a drag coefficient, respectively. This decrease in wind velocity along the flame base has been reported by Anderson *et al.* (2010).

Flame depth L is equal to the product of the R and flame residence time τ ($L = R\ \tau$). In the current formulation flame residence time is estimated from surface area-to-volume ratio ($\tau = \tau_0/s$) as parameterised by Anderson (1969). The modelling of drag forces is slightly modified in order to take into account the whole fuel (live and dead fuel) and the drag coefficient K^* is

assumed to linearly depend on fuel porosity ($K^* = K_1\ s\ \beta_t$) with K_1 is a drag coefficient. So Eqn 17 yields

$$U(L) = U\frac{h}{h+\frac{H}{2}}Exp(-KR) \quad (18)$$

where the drag forces law K is defined as follows:

$$K = \frac{\beta_t}{\min\left(\frac{W_0}{50},1\right)} \quad (19)$$

Note that, contrary to (Balbi *et al.* 2020), the model coefficient K_1 depends on W_0 and thus it is removed from Eqn 19 and is not a model parameter anymore.

Finally, after some simplifications (see Appendix C for further calculus), combining Eqns 4, 15-16 and 18-19 yields

$$R_c = a_M\min\left(\frac{W_0}{50},1\right)\frac{\Delta H\rho_a T_a\, s\sqrt{h}}{2q(s_t+1)\rho_v T}\left(\frac{(s_t+1)}{\tau_0}\frac{\rho_v}{\rho_a}\frac{T}{T_a}\min\left(S,\frac{2\pi S}{S_t}\right)\tan\alpha + U\,Exp\left(-\frac{\beta_t}{\min\left(\frac{W_0}{50},1\right)}R\right)\right) \quad (20)$$

Main equations of the improved model

Combining Eqns 2-4, 8, 9, 15 and 20, the equation (1) of the ROS is written in its detailed expression:

$$R = \min\left(\frac{S_t}{\pi},1\right)\left(\frac{S}{S_t}\right)^2\frac{BT^4}{\beta\rho_v q} + AR\frac{(1+\sin\gamma-\cos\gamma)}{1+\frac{R\cos\gamma}{sr_{00}}} +$$

$$+ a_M\min\left(\frac{W_0}{50},1\right)\frac{\Delta H\rho_a T_a\, s\sqrt{h}}{2q(s_t+1)\rho_v T}\left(\frac{(s_t+1)}{\tau_0}\frac{\rho_v}{\rho_a}\frac{T}{T_a}\min\left(S,\frac{2\pi S}{S_t}\right)\tan\alpha + U\,Exp\left(-\frac{\beta_t}{\min\left(\frac{W_0}{50},1\right)}R\right)\right) \quad (21)$$

where the radiative factor A is defined as following:

$$A = \min\left(\frac{S}{2\pi},\frac{S}{S_t}\right)\frac{\chi_0\Delta H}{4q} \quad (22)$$

Equations for the flame tilt angle γ, flame height H and flame temperature T are not changed since (Balbi *et al.* 2020):

$$\tan\gamma = \tan\alpha + \frac{U}{u_0} \tag{23}$$

$$T = T_a + \frac{\Delta H\,(1-\chi)}{(s_t+1)C_{pa}} \tag{24}$$

$$H = \frac{u_0^2}{g\left(\frac{T}{T_a}-1\right)} \tag{25}$$

Eqns 21-25 can be summed up in one non linear algebraic equation (Eqn 21). As the ROS given in eqn 21 depends on environmental parameters (wind velocity, terrain slope angle, ignition line length, ambient temperature), fuel characteristics (dead FMC, total leaf area, packing ratio, fuel density, surface area-to-volume ratio, heat of combustion of pyrolysis gases, specific heat of fuel) and on the ROS itself, an iterative method is necessary to numerically solve this equation. A convergent series is built in which its first term is the solution of the radiative model defined by Eqn A2 (solution of second order polynomial). Then a loop is performed up to convergence.

Note that Eqn 21 depends on four model parameters: the air-pyrolysis gases mass ratio in the flame body (s_t), a model coefficient (r_{00}), a radiant factor (χ_0) and a fitted model parameter (a_M). Of these all but a_M have been determined by Balbi et al. (2020) and are not expected to vary for the current model parameterization. Parameter a_M needs to be determined for field scale fires. As the various parameter values are assumed to not vary with fuel characteristics in free-spreading shrubland fires, the proposed model is fully predictive.

Data

Two distinct field scale, experimental fire datasets were used in the present analysis. One for model calibration and the other for model evaluation against independent data.

Model calibration

Model calibration for its application to field scale shrubland fires required the estimation of the a_M parameter. This model calibration used the experimental dataset published by Bilgili and Saglam (2003). This series was carried out in a shrubland fuel type (maquis) in Turkey. These authors reported on a study where 25 experimental shrubland fires were conducted on flat ground under a range of weather and fuel conditions. Plot size was 20 x 30 m, for a 20 m ignition line and 30 m run. Wind speed (measured at 1.8 m height) varied between 0.27 m s^{-1} and 4.11 m s^{-1}. Fuel height ranged between 0.35 m and 1.15 m. Fine fuel load for the dead and live components ranged between 0.46 and 0.82 kg m^{-2}, and 0.95 and 1.49 kg m^{-2}, respectively. Rate of fire spread varied between 0.013 and 0.11 m s^{-1}. Further details on environmental conditions are given in the original publication. The estimation of the a_M parameter was based on the parameter that would minimize error and bias.

Sensitivity analysis

A univariate sensitivity (Millington et al. 2009) analysis was conducted to quantify the effect of different fuel parameters on the modelled *R*. This analysis allows to identify the most influential variables in the R ouput. This analysis considers a benchmark simulation on flat ground under a 2 m s^{-1} fuel level wind velocity, 10% dead fuel moisture content and a total fine fuel loading of 0.5 kg m^{-2}. The full list of variables tested in the analysis and their default values is given in Table 2). The sensitivity analysis consists in calculating the percent change in ROS between the benchmark environment and the simulation with the fuel parameter perturbed by plus or minus 10%. This analysis considers the effects of the variable perturbation separately

applied to each fuel characteristic. Note that the perturbation of total fine fuel loading only affects the fine live fuel load because the dead fuel loading of 0.3 kg m^{-2} does not vary.

Model evaluation

The proposed model predictive capacity was evaluated through its application to the data given in (Anderson *et al.* 2015) and (van Wilgen *et al.* 1985). Anderson *et al.* (2015) gathered a large set of experimental field fires from several regions of the world, namely from (New Zealand, Spain, Portugal, Australia and South Africa. The dataset in Anderson *et al*. (2015) provides the necessary detail relative to fire environment and fuel variables that allow the evalution of Eqn (21). Of the 135 fires reported in the Anderson's database (Table A1 in (Anderson *et al.* 2015)), only fires where live fuel data, quantity and moisture content were given (n = 109) were used. This dataset was complemented with the data from 14 experimental fires conducted on fynbos vegetation by van Wilgen *et al.* (1985) in South Africa. This data was used by Anderson *et al*. (2015) but the data not given in their table A1. A usual power law wind profile (Peterson and Hennessey Jr 1978) is used to calculate the wind speed at fuel height necessary to run the proposed model.

Benchmark models used for model fit comparison purposes

To better understand the relevance of the obtained model fit statistics, the evaluation statistics obtained with Eqn 21 are compared to the results obtained using other existent models against the same datasets. The following models were run against the (Anderson *et al.* 2015) dataset (equations of each model are provided in appendix A): (1) a predictive version of the radiative only model presented by Balbi *et al.* (2010) (Eqn A1), (2) the generic shrubland fire spread model provided by Anderson *et al.* (2015) (Eqn A4) and (3) the simplified physical model given by Balbi *et al.* (2020) (Eqn A5). We note that the evaluation data being use here was part of the dataset used to develop the Anderson *et al*. (2015) model.

Statistics used

The error between predicted and measured values is quantified through a number of metrics. To estimate the overall deviations we used the normalized mean square error (NMSE) introduced by Poli and Cirillo (1993). The fractional bias (FB, see (Warner *et al.* 2004)) was used to understand the model's under-predictions or over-predictions trends. This normalized tool makes the bias non-dimensionless. It varies from -2 to +2 and a positive value indicates an overestimated measured value. An ideal model is obtained for an ideal value of zero for NMSE and FB. Residuals (res = predicted R – observed R) and relative error (res/observed R) are also used in the analysis.

Numerical Results

Model calibration

The proposed model (Eqn 21) exhibits four model parameters. The values of three of these parameters (s_t = 16, $r_{00} = 2.5\times10^{-5}$, χ_0 =0.3) are set in (Balbi *et al.* 2020) and do not change in the proposed model. Indeed these three parameters are related to flame radiation whose modelling did not evolved. The a_M parameter was found to be most suitable parameter to parametrize the model for its application against outdoor fires. A value of 0.025 for the a_M parameter leads to the best agreement between the predicted and the observed ROS in (Bilgili and Saglam 2003) dataset (see Fig. 2). This value and the ensuing fit produce a small deviation (NMSE=0.038) without bias (FB=0.00). This parameter is assumed to be a universal coefficient, with its value not changing when applying the model to other field fires, i.e. it is independent of environmental, topographical and fuel conditions.

Model behaviour

315 Fig. 3 illustrates the predicted *R* with changes in some of the most influential environmental
316 variables in shrubland fires, namely wind speed, fuel moisture and fuel height (e.g. (Fernandes
317 *et al.* 2000; Anderson *et al.* 2015)). Benchmark values are given in Table 2.

318 Modelled ROS against wind velocity for 5 different values of the dead fuel load (0.1, 0.15, 0.2,
319 0.25 and 0.3 kg m^2) shows *R* increasing linearly with wind speed (Fig 3a) for the lower fuel
320 loads (0.1 and 0.15 kg m^2). For the higher fuel loads simulated (0.2, 0.25 and 0.3 kg m^2) the
321 model suggests a slow increase of the ROS for low wind speeds and then a faster increase for
322 wind speeds greater than 2.5 m s^{-1}. Fig. 3a also shows that for each value of wind speed, the
323 ROS increases with the dead fuel load but the difference between ROS calculated for two
324 consecutive dead fuel loads tends to decrease with increasing fuel load. This suggests that the
325 model identify the relative influence of fuel load on the ROS to gradually decline with
326 increasing fuel loads. For example, for a 10 m s^{-1} wind speed, the variation of the ROS
327 calculated from consecutive dead fuel loads are 0.12, 0.10, 0.07 and 0.05 m s^{-1}. These
328 simulations assume a constant fuel bed height, with changes in fuel load affecting the fuel layer
329 bulk density, a fuel bed parameter influencing a number of fluid flow and heat transfer
330 efficiencies (Rothermel 1972; Anderson *et al.* 2015). The effect of fuel load, fuel height and
331 bulk density on fire propagation in shrubland vegetation are intimately connected, and it is often
332 difficult, if not impossible, to extract the effect of one variable independently from the effect of
333 the other two in natural fuel beds. We did not explicitly investigate the effect of fuel bulk density
334 on model behaviour in this analysis due to space constraints.

335 The effect of FMC on ROS is presented in Fig. 3b, using the ratio the predicted ROS and an
336 hypothetical ROS for zero FMC (R/ROS(m=0)), as per (Morvan 2013). The observed decay in
337 ROS/ROS(m=0) expressing the relative influence of FMC on ROS follows the trends obtained
338 by Balbi *et al.* (2020), by simulations carried out with FireStar2D (Morvan 2013) and the
339 exponential decay in ROS as a function of FMC modelled by Anderson *et al.* (2015), Fernandes

340 *et al.* (2009) or Rossa *et al.* (2016). As found by Anderson *et al*. (2015), the effect is not
341 pronounced.

342 The influence of fuel bed height on ROS is illustrated in Fig. 3c for four different wind
343 velocities (2.5, 5, 7.5 and 10 m s^{-1}). The ROS is found to increase with fuel height
344 independently of wind speed. A doubling in fuel height from 1 to 2 meters results in a 31%
345 increase on average in *R* but it is noticeable that this increase in the *R* output is more pronounced
346 for low wind speeds (42.8%, 31.4%, 27.3%, 25.2%, for wind speeds of 2.5, 5, 7.5 and 10 m s^{-1}
347 respectively). Results also indicate that the higher the fuel bed height the lower the effect of
348 height increases (whatever the wind speed).

349 *Sensitivity analysis*

350 The univariate sensitivity analysis shows that the fuel characteristics leading to the most
351 important variation in ROS are surface area-to-volume ratio, fuel density, heat of combustion
352 of pyrolysis gases and specific heat (see Table 2). All these variables showed an effect
353 approximately proportional to the 10% perturbation. It is important to notice that these
354 variables, with the exception of surface area-to-volume ratio, tend to be considered constant in
355 fire behaviour modelling. The ±10% change in fuel height and dead fuel moisture content result
356 in an approximate 5% change in the *R* output. Fuel load parameters, dead and total, were the
357 fuel variables showing the least impact on the change in *R*, with the perturbation leading to an
358 absolute percent change varying between 0.8 and 3.5%. These results are restricted to the range
359 of the defaut values used in the sensitivity analysis. A more comprehensive sensitivity analysis
360 over the natural range of the fuel variables tested would likely show areas where the model will
361 be more sensitive to changes in environment conditions.

362 *Model evaluation and comparison*

363 The scatter diagram plotted in Fig. 4a compares predicted and observed ROS for fires conducted
364 in New Zealand (NZ), Australia (WC and SA), Portugal (PT), Spain (SP) and South Africa
365 (SoA). The solid line and dashed lines represent the line of perfect agreement and ±35% error
366 levels, respectively. A good overall agreement is found with an average NMSE of 0.132 and a
367 slight under-estimation of the predicted ROS (FB=-0.03). Larger relative errors presented in
368 Fig. 4c seem to concentrate in the lower rates of fire spread. Table 3 displays the full model
369 performance results for each experimental series. It is noticeable that deviation results are very
370 low (NMSE close to 0) for all the experimental fire series, with the exception of the Portugal
371 fire dataset that yield a NMSE of 0.308. Fig. 4c illustrates behaviour with the Portugal fires
372 subset showing the largest relative error of all data subsets. Fig. 5a and b plot residuals and
373 relative error as a function of observed ROS in four broad classes. The residual distribution
374 shows the model to produce unbiased results within the three lower R classes (R< 0.5 m s^{-1}) and
375 a higher under-prediction for the faster spreading fires (R > 0.5 m s^{-1}). The analysis of the
376 percent error shows that this increase in residuals for faster fires is associated with the lowest
377 percent errors (Fig. 5b). The model error in a relative sense decreases considerably as the
378 observed R increases.

379 *Analysis of modelled convective and radiative heat transfer*

380 The bubble diagram (Fig. 6) plots the convective (R_c, Eqn 3) *v.* radiative (R_b+R_r, Eqns 2 and 4)
381 contributions calculated on the datasets of Anderson *et al.* (2015) and Bilgili and Saglam
382 (2003). Wind speed is the third variable and the larger the bubble sizes, the larger the wind
383 speed. The solid line represents the perfect equilibrium between these two contributions. Fig. 6
384 shows the model identifying convection as the main heat transfer mechanism for 79.7% of the
385 fires (118 of 148). Radiation is identified as dominant in all the 10 fires of one of the Australia
386 fire group (SA). If convection is found to drive all the South African (SoA), Turkish (TU) and
387 Australian (WC), the convective contribution to the ROS also outweighs the radiative effects

388 in the major part of New Zealander (NZ), Portuguese (PT) and Spanish (SP) fires (89.2%,
389 79.2% and 72.73% respectively). So, overall, the model formulation identified convection as
390 the most influential heat transfer mechanism driving fire propagation. As an exception, two
391 Spanish fires burning under nil, or zero, wind conditions had radiative heat transfer largely
392 dominating fire propagation.

393 *Comparison with other models*

394 The comparison of model fit statistics obtained with the eqn 21 model and previous published
395 models is presented in Table 3. The Balbi *et al*. (2010) radiative model yields the largest NMSE
396 and a strong underestimation. The results obtained by the Anderson *et al.* (2015) empirical
397 model (NMSE=0.180, FB=-0.05) were expected to a good approximation of the observed ROS
398 as the data used in this evaluation was part of the data used in the development of the model
399 (Eqn A4). The Balbi *et al.* (2020) model also produced very encouraging results, with an overall
400 NMSE of 0.183 and a FB of -0.02. This corroborates Balbi *et al*. (2020) claims that their model
401 could be used at field scale even if it was developed at laboratory scale. Overall, the eqn 21
402 model produced the best results of all the models analysed, with small overall deviations
403 (NMSE=0.132) and a bias close to zero (FB=-0.03). Fig. 7 presents the comparison between
404 the previous models as a scatter plot; the Balbi *et al* (2010) radiative model was removed from
405 this plot because of its poor agreement with observed data.

406 ## Discussion

407 *Effect of domimant environmental variables*

408 The proposed model produces a quasi-linear relationship between R and wind speed, with the
409 increase in wind speed resulting in an increase in R following expectations from laboratory and
410 field observations (Bilgili and Saglam 2003; Mendes-Lopes *et al.* 2003; Butler *et al.* 2019). The

411 wind speed effect depends on other fuel characteristics, due to the effect of structural fuel
412 characteristics on heat transfer processes. As example, fuel load affects the radiative coefficient
413 (0.1 and 0.15 kg m^{-2} lead to A=0.27 and A=0.41, respectively), and this effect is dependent on
414 wind speed as well. The linear (when $A < ½$) or quasi-linear ($A > ½$) ROS trend agrees with
415 experimental results presented by Beer (1991) on match splints, Rothermel and Anderson
416 (1966) on ponderosa pine and white pine needles fuel beds or Cheney *et al.* (1993) on grass
417 fuel (where the exponent modelling the effect of wind speed on ROS, $R \propto aU^b$ is close to 1).

418 At zero wind speed, both the convective effects and the radiative contribution from the flame
419 body are nil (on flat ground) or close to zero (on sloped ground) and the fire is driven by the
420 flame base radiation (R_b). As wind speed U increases, the convective (R_c) and radiative (R_r)
421 contributions increase as well, directly through U in R_c (Eqn 20) and through the increasing
422 flame tilt angle for R_r (Eqn 23). Note that if R_r is always an increasing function of the wind
423 speed, R_c theoretically increases with wind speed up to a threshold wind speed value because
424 of the exponential in its definition. This threshold value is difficult to assess but it is quite an
425 extreme value of the wind speed. As example, selecting the ROS obtained in the numerical
426 simulations for a dead fuel load of 0.2 kg m^{-2}, R_c increases from 0 to 0.65 m s^{-1}, which means
427 that the threshold value is not reached, even for a 25 m s^{-1} wind speed.

428 The model suggests an effect of fuel height on R to be dependent on other fire environmental
429 variables. For low wind speeds a doubling in fuel height results in an approximately 50%
430 increase in R, as found in the univariate sensitivity analysis. The same doubling in fuel height
431 at high wind speeds can result in a 25 to 35% increase in R. The effect captured by the model
432 is comparable to the effect captured by Anderson et al. (2015) model. Nonetheless, the physics
433 nature of the proposed model allowed to captured a more nuanced effect as influenced by other
434 environmental and fuel conditions. It is noticeable that the most sensitive fuel characteristics
435 for the proposed model are intrinsic fuel properties (fuel characteristics directly related to the

436 fuel species). Nonetheless, it should be noticed that these intrinsic fuel characteristics vary
437 within a narrow range comparatively to the range in structural variables such as fuel load or
438 fuel height. Our results also show that the sensitivity of the model to the variation in the extrinsic
439 fuel characteristics (FMC, height and load) does not cause large errors on the ROS output. This
440 is encouraging from the point of view that within an operational fire simulation setting, an error
441 in these estimates leads to a controlled error on the ROS.

442 *Model predictive performance*

443 The overall comparison between predicted and observed ROS on the Anderson's dataset leads
444 to a NMSE of 0.132 with a bias close to zero (FB=-0.03). We consider this to be a very good
445 result for the application of fire spread models at a field scale, especially when the model was
446 applied to shrubland fires from different sources and covering a broad range of fuel structures.
447 The results showed that the model performance was worse for the dataset of Portuguese fires,
448 where the NMSE was more than doubled the average NMSE for all fires. This result was
449 observed in (Anderson *et al.* 2015) analysis, with the Portugal fire subset showing a distinct
450 dynamics than the remaining data. The source of this differences was unclear to Anderson *et*
451 *al.* (2015).

452 Our results suggest the model relative accuracy to increase with an increase in observed rate of
453 spread, or severity of burning conditions. For a model designed to be used operationally, errors
454 in the slow spreading fires are somewhat inconsequential. The reduction in relative error for
455 the fast spreading fires ensures the model can be better trusted under operational conditions
456 where simulations for these type of fires are most needed.

457 Overall, the good agreement between predicted and observed ROS presented by the proposed
458 model, with errors comparable but slightly lower than obtained with Anderson *et al*. (2015)
459 model, suggests that it is qualified to be used to predict the propagation of shrubland fires in an

operational setting. The current formulation predicted shrubland fire spread more accurately than the radiative model derived from (Balbi *et al.* 2010) which has been implemented in the Forefire simulator (Filippi *et al.* 2011).

Heat transfer mode

The relative contribution of the convective and radiative heat transfer to the ROS was also analysed. The ratio of convective to radiative heat transfer for the experimental shrubland fires used in model evaluation was above 1 for 79.7% of the fires, implying convection to be the dominant heat transfer mode in these fires. These results agree with the simulations conducted by Morvan and Dupuy (2004) on mediterranean shrubs. The convection dominance is more pronounced when the model is tested against the NZ data which present the higher wind speeds and high fuel loads. The same effect is found for the South African fires which has the second higher wind speed average of the whole dataset. So convection seems to be more dominant with high wind speeds. This trend agrees with the main tendencies provided by detailed physical models such as FireStar3D (Morvan *et al.* 2018) in which convection increases with wind speed. It was expected because of the definition of the ROS in the model (Eqn 21) in which the convective contribution linearly depends on wind speed. But according to the ROS expression of the proposed model, an increasing ROS reduces the value of the exponential in Eqn 21 and very fast ROS will finally cause a decreasing convective contribution to the ROS. This decrease happens for extreme wind speed values (no decrease was found in the numerical simulations performed under wind speeds up to 25 m s^{-1}). Radiation prevails in all the fires of the Australian (SA) group which are conducted in a semi-arid environment (smaller average dead and live FMC and low fuel loads). Radiation is also dominant for fires spreading under zero wind conditions because the convective contribution is zero (Eqn 21) and the ROS is mainly driven by the flame base radiation ($R = R_b$).

Conclusion

This work deals with the adaptation of the Balbi *et al.* (2020) convective-radiative surface fire propagation model originally developed to describe laboratory scale fires, to fires propagating at a field scale in shrubland fuels. The improved model is a simplified physical model which takes into account convective and radiative effects as heat transfer mechanisms and is designed to allow its application under operational conditions. The main physical characteristics of the fire front are assessed through algebraic equations. The ROS is calculated using a non-linear algebraic equation solved through an iterative method. It depends on environmental (wind velocity, ambient temperature), topographical (terrain slope angle) conditions and a number of intrinsic and extrinsic fuel characteristics (e.g. FMC, thickness, packing ratio, surface area to volume ratio, dead and live fuel load). The living part of the fuel is mainly taken into account through the contribution of live fuel load.

Like other simplified physical models, the improved model is not able to use a detailed description of the fuel complex when the available biomass is composed of multiple species or layers with distinct physical structures, it needs an equivalent idealized fuel description in order to be run.

The level of detail in the physical conservation laws, the low computational cost (faster than real time) and the observed good agreement obtained against independent data are encouraging results obtained in the present work. With model parameterization requiring only a restricted number of experimental fires, the model framework has potential to be extended to different fuel types such as grasslands and conifer forests, by using existent datasets. The model can be implemented in fire spread simulators such as ForeFire (Filippi *et al.* 2011) and it is currently being tested within the couple atmosphere-fire model WRF-Sfire (Kochanski *et al.* 2013).

Conflict of Interest

The authors declare they have no conflicts of interest.

Acknowledgements

The present work was supported in part by the Corsican Region under Grant GOLIAT 2020–2023. The authors also wish to thank Dr. E. Bilgili for sharing its corrected data on his field experiments.

References

Albini FA (1985) A Model for Fire Spread in Wildland Fuels by-Radiation. *Combustion Science and Technology* **42**, 229–258. doi:10.1080/00102208508960381.

Albini FA (1986) Wildland Fire Spread by Radiation - a Model Including Fuel Cooling by Natural Convection. *Combustion Science and Technology* **45**, 101–113.

Anderson HE (1969) Heat transfer and fire spread. (U.S. Department of Agriculture, Forest Service, Research Paper INT-69)

Anderson WR, Catchpole EA, Butler BW (2010) Convective heat transfer in fire spread through fine fuel beds. *International Journal of Wildland Fire* **19**, 284–298. doi:10.1071/WF09021.

Anderson WR, Cruz MG, Fernandes PM, McCaw L, Vega JA, Bradstock RA, Fogarty L, Gould J, McCarthy G, Marsden-Smedley JB, Matthews S, Mattingley G, Pearce HG, Van Wilgen BW (2015) A generic, empirical-based model for predicting rate of fire spread in shrublands. *International Journal of Wildland Fire* **24**, 443–460. doi:10.1071/WF14130.

Andrews PLPP (1986) BEHAVE: Fire Behavior Prediction and Fuel Modeling System - BURN Subsystem, Part 1. (Ogden, UT 84401) http://digitalcommons.usu.edu/barkbeetles/151/.

529 Balbi JH, Chatelon FJ, Morvan D, Rossi JL, Marcelli T, Morandini F (2020) A convective–
530 radiative propagation model for wildland fires. *International Journal of Wildland Fire* **29**,
531 723–738. doi:10.1071/WF19103.

532 Balbi J-H, Morandini F, Silvani X, Filippi JB, Rinieri F (2009) A physical model for wildland
533 fires. *Combustion and Flame* **156**, 2217–2230. doi:10.1016/j.combustflame.2009.07.010.

534 Balbi J-H, Rossi J-L, Marcelli T, Chatelon F-J (2010) Physical Modeling of Surface Fire Under
535 Nonparallel Wind and Slope Conditions. *Combustion Science and Technology* **182**, 922–
536 939. http://www.tandfonline.com/doi/abs/10.1080/00102200903485178.

537 Balbi J-H, Rossi J-L, Marcelli T, Santoni P-A (2007) A 3D Physical Real-Time Model of
538 Surface Fires Across Fuel Beds. *Combustion Science and Technology* **179**, 2511–2537.
539 http://dx.doi.org/10.1080/00102200701484449
540 http://www.tandfonline.com/doi/pdf/10.1080/00102200701484449.

541 Beer T (1991) The interaction of wind and fire. *Boundary-Layer Meteorology* **54**, 287–308.
542 doi:10.1007/BF00183958.

543 Bilgili E, Saglam B (2003) Fire behavior in maquis fuels in Turkey. *Forest Ecology and*
544 *Management* **184**, 201–207. doi:10.1016/S0378-1127(03)00208-1.

545 Butler B, Quarles S, Standohar-Alfano C, Morrison M, Jimenez D, Sopko P, Wold C, Bradshaw
546 L, Atwood L, Landon J, O'Brien J, Hornsby B, Wagenbrenner N, Page W (2019)
547 Exploring fire response to high wind speeds: Fire rate of spread, energy release and flame
548 residence time from fires burned in pine needle beds under winds up to 27 m s-1.
549 *International Journal of Wildland Fire* **29**, 81–92. doi:10.1071/WF18216.

550 Castro Rego FMC, Moreno Rodriguez JM, Vallejo Calzada VR, Xanthopoulos G (2018) Forest
551 Fires - Sparking firesmart policies in the EU (Nicolas Faivre, Ed.). Publications Office of

552 the European Union, (Luxembourg) doi:10.2777/181450.

553 Catchpole WR, Catchpole EA, Butler BW, Rothermel RC, Morris GA, Latham DJ (1998) Rate
554 of Spread of Free-Burning Fires in Woody Fuels in a Wind Tunnel. *Combustion Science*
555 *and Technology* **131**, 1–37. doi:10.1080/00102209808935753.

556 Chandler C, Cheney P, Thomas P, Trabaud L, Williams D (1983) 'Fire in forestry. Volume 1.
557 Forest fire behavior and effects. Volume 2. Forest fire management and organization.'
558 (John Wiley & Sons, Inc.: New York, NY, USA)

559 Chatelon FJ, Balbi JH, Morvan D, Rossi JL, Marcelli T (2017) A convective model for
560 laboratory fires with well-ordered vertically-oriented fuel beds. *Fire Safety Journal* **90**,
561 54–61. doi:10.1016/j.firesaf.2017.04.022.

562 Cheney N, Gould J (1995) Fire Growth in Grassland Fuels. *International Journal of Wildland*
563 *Fire* **5**, 237–247. doi:https://doi.org/10.1071/WF9950237.

564 Cheney NP, Gould JS, Catchpole WR (1993) The Influence Of Fuel, Weather And Fire Shape
565 Variables On Fire-Spread In Grasslands. *International Journal of Wildland Fire* **3**, 31–44.
566 doi:10.1071/WF9930031.

567 Cheney NP, Gould JS, Catchpole WR (1998) Prediction of fire spread in grasslands.
568 *International Journal of Wildland Fire* **8**, 1–13. doi:10.1071/WF9980001.

569 Cruz MG, McCaw WL, Anderson WR, Gould JS (2013) Fire behaviour modelling in semi-arid
570 mallee-heath shrublands of southern Australia. *Environmental Modelling and Software* **40**,
571 21–34. doi:10.1016/j.envsoft.2012.07.003.

572 Dupuy J-L, Fargeon H, Martin-StPaul N, Pimont F, Ruffault J, Guijarro M, Hernando C,
573 Madrigal J, Fernandes P (2020) Climate change impact on future wildfire danger and

574 activity in southern Europe: a review. *Annals of Forest Science* **77**, 24.
575 doi:10.1007/s13595-020-00933-5.

576 European Science & Technology Advisory Group (2020) Evolving Risk of Wildfires in Europe
577 - The changing nature of wildfire risk calls for a shift in policy focus from suppression to
578 prevention. (Brussels, Belgium) https://www.undrr.org/publication/evolving-risk-
579 wildfires-europe-thematic-paper-european-science-technology-advisory.

580 Fernandes PAM (2001) Fire spread prediction in shrub fuels in Portugal. *Forest Ecology and*
581 *Management* **144**, 67–74. doi:10.1016/S0378-1127(00)00363-7.

582 Fernandes PM (2013) Fire-smart management of forest landscapes in the Mediterranean basin
583 under global change. *Landscape and Urban Planning* **110**, 175–182.
584 doi:10.1016/j.landurbplan.2012.10.014.

585 Fernandes PM, Botelho HS, Rego FC, Loureiro C (2009) Empirical modelling of surface fire
586 behaviour in maritime pine stands. *International Journal of Wildland Fire* **18**, 698–710.
587 doi:10.1071/WF08023.

588 Fernandes PM, Catchpole WR, Rego FC (2000) Shrubland fire behaviour modelling with
589 microplot data. *Canadian Journal of Forest Research-Revue Canadienne De Recherche*
590 *Forestiere* **30**, 889–899. doi:DOI 10.1139/cjfr-30-6-889.

591 Filippi JB, Bosseur F, Pialat X, Santoni PA, Strada S, Mari C (2011) Simulation of coupled
592 fire/atmosphere interaction with the MesoNH-ForeFire models. *Journal of Combustion*
593 **2011**,. doi:10.1155/2011/540390.

594 Finlay SE, Moffat A, Gazzard R, Baker D, Murray V (2012) Health impacts of wildfires. *PLoS*
595 *Currents* **4**, e4f959951cce2c. doi:10.1371/4f959951cce2c.

596 Finney MA (1998) FARSITE: Fire Area Simulator - Model Development and Evaluation.
597 doi:10.2737/RMRS-RP-4.

598 Finney MA, Forthofer J, Grenfell IC, Adam BA, Akafuah NK, Saito K (2013) A study of flame
599 spread in engineered cardboard fuelbeds: Part I: Correlations and observations. In 'Proc.
600 Seventh Int. Symp. Scale Model.', Hirosaki, Japan.(Hirosaki, Japan)

601 Frangieh N, Morvan D, Meradji S, Accary G, Bessonov O (2018) Numerical simulation of
602 grassland fires behavior using an implicit physical multiphase model. *Fire Safety Journal*
603 **102**, 37–47. doi:10.1016/j.firesaf.2018.06.004.

604 Grishin AM (1997) 'Mathematical Modeling of Forest Fires and New Methods of Fighting
605 Them.' (FA Albini, Ed.). (Publishing House of the Tomsk University: Tomsk, Russia)
606 https://books.google.fr/books?id=MtScGwAACAAJ.

607 Hammer RB, Radeloff VC, Fried JS, Stewart SI (2007) Wildland–urban interface housing
608 growth during the 1990s in California, Oregon, and Washington. *International Journal of*
609 *Wildland Fire* **16**, 255. doi:10.1071/WF05077.

610 Keane RE (2019a) Fire Ecology (SL Manzello, Ed.). *Encycl. ofWildfires Wildland-Urban*
611 *Interface Fires* **37**, 350–353. doi:10.1007/978- 3- 319- 51727- 8_254- 1.

612 Keane RE (2019b) LAI : Leaf Area Index (SL Manzello, Ed.). *Encycl. ofWildfires Wildland-*
613 *Urban Interface Fires* 8. doi:https://doi.org/10.1007/978- 3- 319- 51727- 8_237- 1.

614 Keane RE, Drury SA, Karau EC, Hessburg PF, Reynolds KM (2010) A method for mapping
615 fire hazard and risk across multiple scales and its application in fire management.
616 *Ecological Modelling* **221**, 2–18. doi:10.1016/j.ecolmodel.2008.10.022.

617 Kochanski AK, Jenkins MA, Mandel J, Beezley JD, Clements CB, Krueger S (2013) Evaluation

618 of WRF-SFIRE performance with field observations from the FireFlux experiment.
619 *Geoscientific Model Development* **6**, 1109–1126. doi:10.5194/gmd-6-1109-2013.

620 Koo E, Pagni P, Woycheese J, Stephens S, Weise D, Huff J (2005) A simple physical model
621 for forest fire spread rate. *Fire Safety Science* **8**, 854–862. doi:10.3801/IAFSS.FSS.8-851.

622 Lattimer BY (2019) Heat Transfer from Fires (SL Manzello, Ed.). *Encycl. Wildfires Wildland-*
623 *Urban Interface Fires* 1–10. doi:10.1007/978-3-319-51727-8_38-1.

624 Linn RR, Cunningham P (2005) Numerical simulations of grass fires using a coupled
625 atmosphere-fire model: Basic fire behavior and dependence on wind speed. *Journal of*
626 *Geophysical Research Atmospheres* **110**, 1–19. doi:10.1029/2004JD005597.

627 Mandel J, Beezley JD, Kochanski AK (2011) Coupled atmosphere-wildland fire modeling with
628 WRF 3.3 and SFIRE 2011. *Geoscientific Model Development* **4**, 591–610.
629 doi:10.5194/gmd-4-591-2011.

630 McArthur AG (1966) 'Weather and grassland fire behaviour.' (Australia. Forestry and Timber
631 Bureau: Canberra)

632 McCaffrey B (1979) Purely buoyant diffusion flames: some experimental results, NBSIR 79-
633 1910. doi:NBSIR 79-1910.

634 Mell W, Jenkins MA, Gould J, Cheney P (2007) A physics-based approach to modelling
635 grassland fires. *International Journal of Wildland Fire* **16**, 1–22. doi:10.1071/WF06002.

636 Mendes-Lopes JMC, Ventura JMP, Amaral JMP (2003) Flame characteristics, temperature–
637 time curves, and rate of spread in fires propagating in a bed of Pinus pinaster needles.
638 *International Journal of Wildland Fire* **12**, 67–84. doi:10.1071/WF02063.

639 De Mestre NJ, Catchpole EA, Anderson DH, Rothermel RC (1989) Uniform Propagation of a

640 Planar Fire front Without Wind. *Combustion Science and Technology* **65**, 231–2444.
641 doi:10.1080/00102208908924051.

642 Meyer V, Becker N, Markantonis V, Schwarze R, van den Bergh JCJM, Bouwer LM, Bubeck
643 P, Ciavola P, Genovese E, Green C, Hallegatte S, Kreibich H, Lequeux Q, Logar I,
644 Papyrakis E, Pfurtscheller C, Poussin J, Przyluski V, Thieken AH, Viavattene C (2013)
645 Review article: Assessing the costs of natural hazards – state of the art and knowledge
646 gaps. *Natural Hazards and Earth System Sciences* **13**, 1351–1373. doi:10.5194/nhess-13-
647 1351-2013.

648 Morvan D (2013) Numerical study of the effect of fuel moisture content (FMC) upon the
649 propagation of a surface fire on a flat terrain. *Fire Safety Journal* **58**, 121–131.
650 doi:10.1016/j.firesaf.2013.01.010.

651 Morvan D, Accary G, Meradji S, Frangieh N, Bessonov O (2018) A 3D physical model to study
652 the behavior of vegetation fires at laboratory scale. *Fire Safety Journal* **101**, 39–52.
653 doi:10.1016/J.FIRESAF.2018.08.011.

654 Morvan D, Dupuy JL (2004) Modeling the propagation of a wildfire through a Mediterranean
655 shrub using a multiphase formulation. *Combustion and Flame* **138**, 199–210.
656 doi:10.1016/j.combustflame.2004.05.001.

657 Morvan D, Dupuy JL, Porterie B, Larini M (2000) Multiphase formulation applied to the
658 modeling of fire spread through a forest fuel bed. *Proceedings of the Combustion Institute*
659 **28**, 2803–2809. doi:10.1016/S0082-0784(00)80702-X.

660 Morvan D, Méradji S, Accary G (2009) Physical modelling of fire spread in Grasslands. *Fire*
661 *Safety Journal* **44**, 50–61. doi:10.1016/j.firesaf.2008.03.004.

662 Nelson Jr. RM, Adkins CW (1986) Flame characteristics of wind-driven surface fires.

663 *Canadian Journal of Forest Research* **16**, 1293–1300. doi:10.1139/x86-229.

664 Noble IR, Gill AM, Bary GAV (1980) McArthur's fire-danger meters expressed as equations.
665 *Australian Journal of Ecology*. doi:10.1111/j.1442-9993.1980.tb01243.x.

666 Pagni PJ, Peterson TG (1973) Flame spread through porous fuels. *Symposium (International)*
667 *on Combustion* **14**, 1099–1107. doi:10.1016/S0082-0784(73)80099-2.

668 Pastor E, Zárate L, Planas E, Arnaldos J (2003) Mathematical models and calculation systems
669 for the study of wildland fire behaviour. *Progress in Energy and Combustion Science* **29**,
670 139–153. doi:10.1016/S0360-1285(03)00017-0.

671 Perry GLW (1998) Current approaches to modelling the spread of wildland fire: a review.
672 *Progress in Physical Geography* **22**, 222–245. doi:10.1177/030913339802200204.

673 Peterson EW, Hennessey Jr JP (1978) On the use of power laws for estimates of wind power
674 potential. *Jurnal of applied meteorlogy* **17**, 390–394.

675 Pimont F, Ruffault J, Martin-StPaul NK, Dupuy JL (2019) Why is the effect of live fuel
676 moisture content on fire rate of spread underestimated in field experiments in shrublands?
677 *International Journal of Wildland Fire* **28**, 127–137. doi:10.1071/WF18091.

678 Poli AA, Cirillo MC (1993) On the use of the normalized mean square error in evaluating
679 dispersion model performance. *Atmospheric Environment Part A, General Topics* **27**,
680 2427–2434. doi:10.1016/0960-1686(93)90410-Z.

681 Radeloff VC, Hammer RB, Stewart SI, Fried JS, Holcomb SS, Mckeefry JF (2005) The
682 Wildland–Urban Interface in the United States. *Communications Ecological Applications*
683 **15**, 799–805. doi:10.1890/04-1413.

684 Rossa CG, Fernandes PM (2018) An Empirical Model for the Effect of Wind on Fire Spread

685 Rate. *Fire 2018, Vol 1, Page 31* **1**, 31. doi:10.3390/FIRE1020031.

686 Rossa CG, Veloso R, Fernandes PM (2016) A laboratory-based quantification of the effect of
687 live fuel moisture content on fire spread rate. *International Journal of Wildland Fire* **25**,
688 569–573. doi:10.1071/WF15114.

689 Rothermel RC (1972) A mathematical model for predicting fire spread in wildland fuels.
690 (USDA Forest Service, Research Paper INT-115, Intermountain Forest and Range
691 Experiment Station, Ogden, Utah)
692 doi:http://www.snap.uaf.edu/webshared/JenNorthway/AKFireModelingWorkshop/AKFi
693 reModelingWkshp/FSPro Analysis Guide References/Rothermel 1972 INT-115.pdf.

694 Rothermel RC, Anderson HE (1966) Fire spread characteristics determined in the laboratory.
695 (USDA Forest Service, Research Paper INT-30, Intermountain Forest and Range
696 Experiment Station, Ogden, Utah)

697 Running SW (2006) Is Global Warming causing more, large wildfires. *Science* **313**, 927–928.
698 doi:10.1126/science.1130370.

699 Sağlam B, Bilgili E, Küçük Ö, Dinç Durmaz B (2008) Fire behavior in Mediterranean shrub
700 species (Maquis). *African Journal of Biotechnology* **7**, 4122–4129.
701 doi:10.5897/AJB08.782.

702 San-Miguel-Ayanz J, Moreno JM, Camia A (2013) Analysis of large fires in European
703 Mediterranean landscapes: Lessons learned and perspectives. *Forest Ecology and*
704 *Management* **294**, 11–22. doi:10.1016/j.foreco.2012.10.050.

705 Sullivan AL (2009a) Wildland surface fire spread modelling, 1990–2007. 1: Physical and quasi-
706 physical models. *International Journal of Wildland Fire* **18**, 349–368.
707 doi:10.1071/WF06144.

708 Sullivan AL (2009b) Wildland surface fire spread modelling, 1990–2007. 2: Empirical and
709 quasi-empirical models. *International Journal of Wildland Fire* **18**, 369–386.
710 doi:10.1071/WF06144.

711 Sullivan AL (2009c) Wildland surface fire spread modelling, 1990–2007. 3: Simulation and
712 mathematical analogue models. *International Journal of Wildland Fire* **18**, 387–403.
713 doi:10.1071/WF06144.

714 Tang Y, Zhong SY, Luo LF, Bian XD, Heilman WE, Winkler J (2015) The Potential Impact of
715 Regional Climate Change on Fire Weather in the United States. *Annals of the Association*
716 *of American Geographers* **105**, 1–21. doi:Doi 10.1080/00045608.2014.968892.

717 Viegas DX (2004) Slope and wind effects on fire propagation. *International Journal of*
718 *Wildland Fire* **13**, 143–156. doi:10.1071/WF03046.

719 Warner S, Platt N, Urban JT, Heagy JF (2004) Comparisons of transport and dispersion model
720 predictions of the joint urban 2003 field experiment. *Journal of Applied Meteorology* **43**,
721 829–846. doi:10.1175/2007JAMC1802.1.

722 Weber RO (1991) Modelling fire spread through fuel beds. *Prog. Energy Combust. Sci.* **17**, 67–
723 82. doi:10.1016/0360-1285(91)90003-6.

724 Weise DR, Koo E, Zhou X, Mahalingam S, Morandini F, Balbi JH (2016) Fire spread in
725 chaparral - A comparison of laboratory data and model predictions in burning live fuels.
726 *International Journal of Wildland Fire* **25**, 980–994. doi:10.1071/WF15177.

727 van Wilgen BW, Le Maitre DC, Kruger FJ (1985) Fire behaviour in South African
728 fynbos(macchia) vegetation and predictions from Rothermel's fire model. *Journal of*
729 *Applied Ecology* **22**, 207–216. doi:10.2307/2403338.

730 Wolff MF, Carrier GF, Fendell FE (1991) Wind-aided firespread across arrays of discrete fuel
731 elements. II. Experiment. *Combustion Science and Technology* **77**, 261–289.
732 doi:10.1080/00102209108951731.

733 Wotton BM, Martell DL, Logan KA (2003) Climate change and people-caused fire occurrence
734 in Ontario. *Climatic Change* **60**, 275–295. doi:10.1023/A:1026075919710.

735 Youssouf H, Liousse C, Roblou L, Assamoi E-M, Salonen R, Maesano C, Banerjee S, Annesi-
736 Maesano I (2014) Non-Accidental Health Impacts of Wildfire Smoke. *International*
737 *Journal of Environmental Research and Public Health* **11**, 11772–11804.
738 doi:10.3390/ijerph111111772.

739

The manuscript proposes an extension of the Balbi model to the field scale. In addition to the necessary modelling section, we made a comparison between the results obtained with the proposed model and more than 100 experimental shrubland fires picked up in the literature. As the previous version of the Balbi model (developed at the laboratory scale) was published in IJWF (2020), and due to the very interesting comments from the fire community we received, we believe that the IJWF is the most appropriate outlet for the present manuscript given its broad reach to an operational and scientific readership.

The main interest of this work is to propose a simplified physical model designed to be used under operational conditions. The model takes explicitly into account the triangle of fire (wind, slope and main fuel characteristics), is fully predictive, faster than real time and can be easily used at the field scale with a good accuracy.

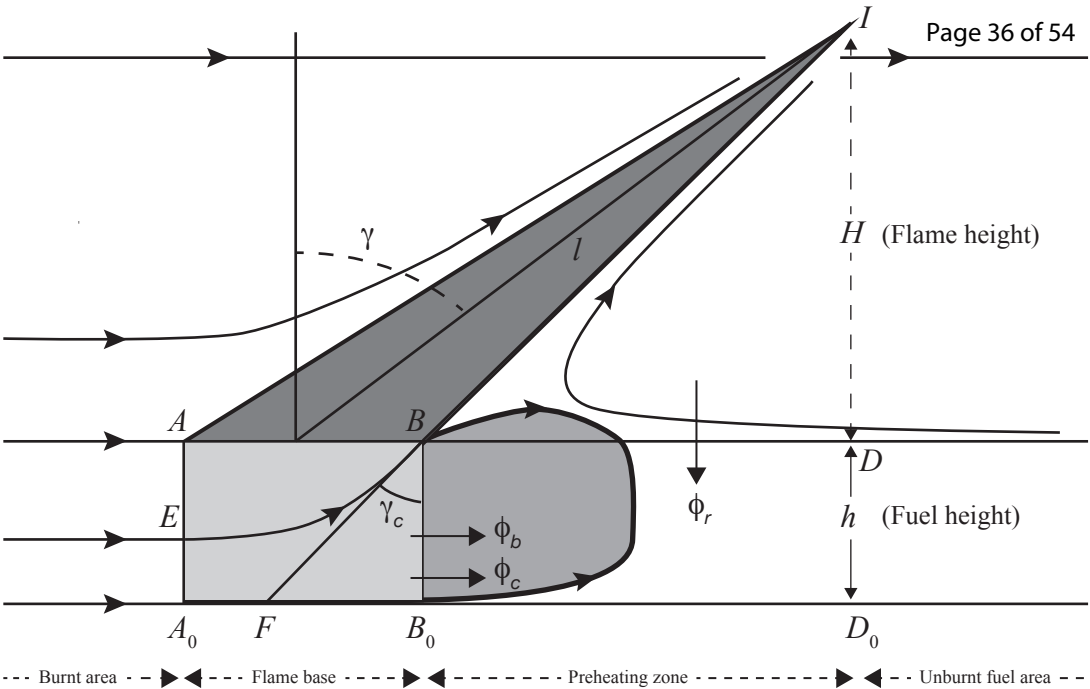
I
H (Flame height)
γ
l
A
B
D
E
γc
ϕb
ϕc
ϕr
h (Fuel height)
A0
F
B0
D0
Burnt area
Flame base
Pyrolysis area
Preheating zone
Unburnt fuel area

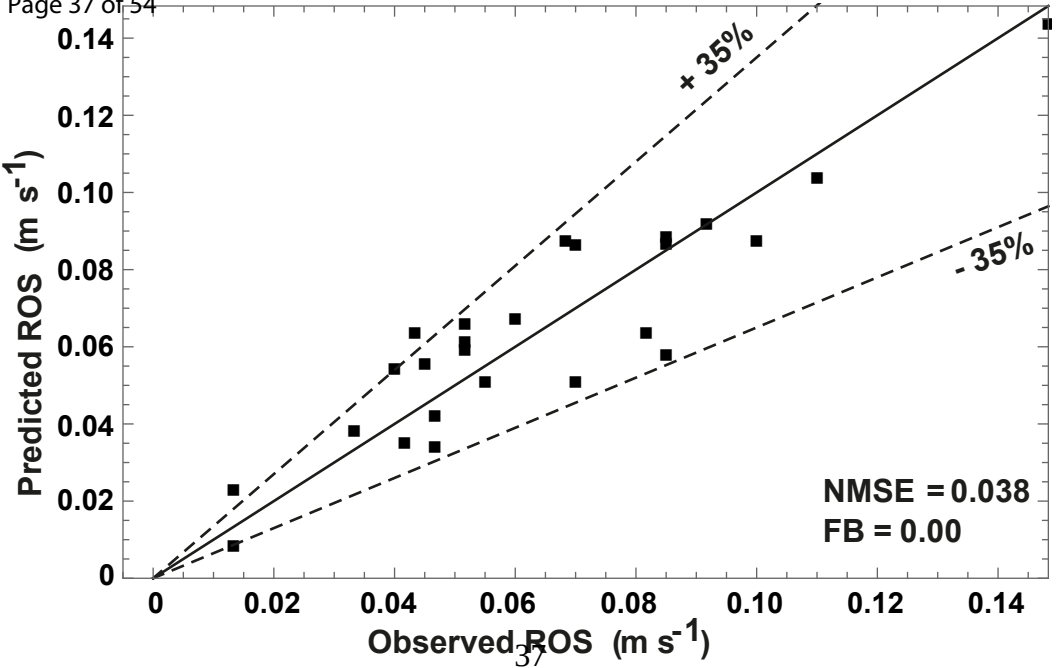
Predicted ROS (m s-1)
Observed ROS (m s-1)
0
0.02
0.04
0.06
0.08
0.10
0.12
0.14
+ 35%
- 35%
NMSE = 0.038
FB = 0.00

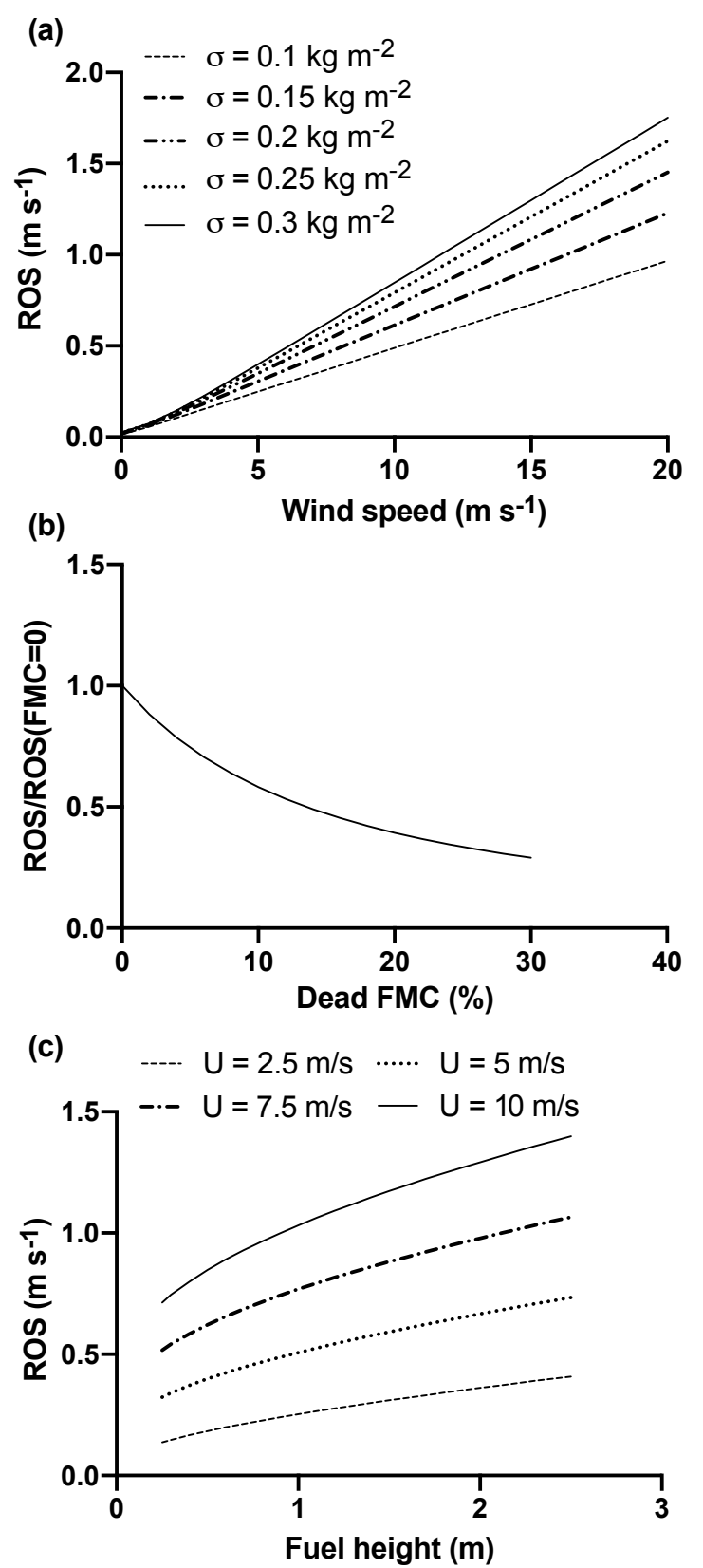
(a)
σ = 0.1 kg m-2
σ = 0.15 kg m-2
σ = 0.2 kg m-2
σ = 0.25 kg m-2
σ = 0.3 kg m-2
ROS (m s-1)
2.0
1.5
1.0
0.5
0.0
0
5
10
15
20
Wind speed (m s-1)
(b)
ROS/ROS(FMC=0)
1.5
1.0
0.5
0.0
0
10
20
30
40
Dead FMC (%)
(c)
U = 2.5 m/s
U = 5 m/s
U = 7.5 m/s
U = 10 m/s
ROS (m s-1)
1.5
1.0
0.5
0.0
0
1
2
3
Fuel height (m)

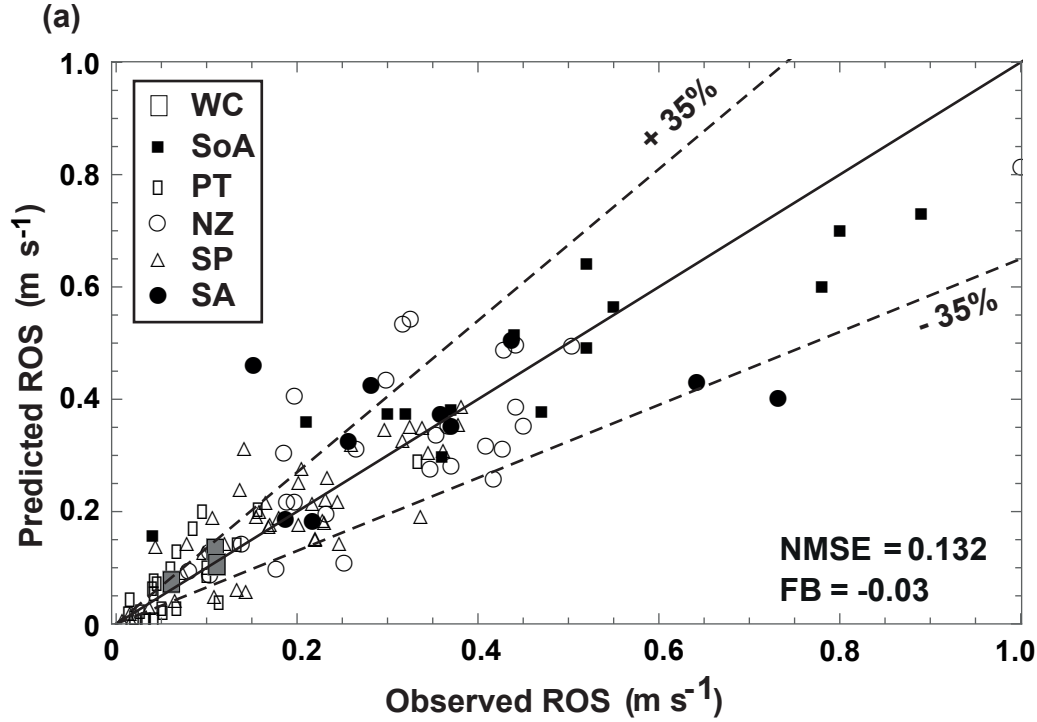
(a)
WC
SoA
PT
NZ
SP
SA
+ 35%
- 35%
NMSE = 0.132
FB = -0.03
Predicted ROS (m s-1)
Observed ROS (m s-1)
0
0.2
0.4
0.6
0.8
1.0

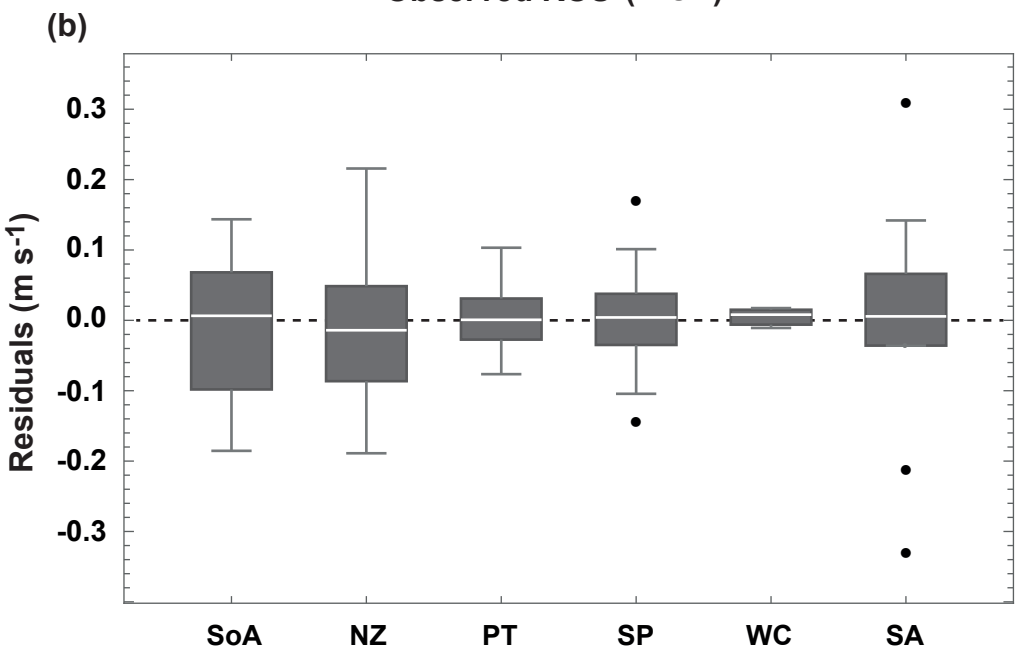
(b)
Residuals (m s-1)
0.3
0.2
0.1
0.0
-0.1
-0.2
-0.3
SoA
NZ
PT
SP
WC
SA

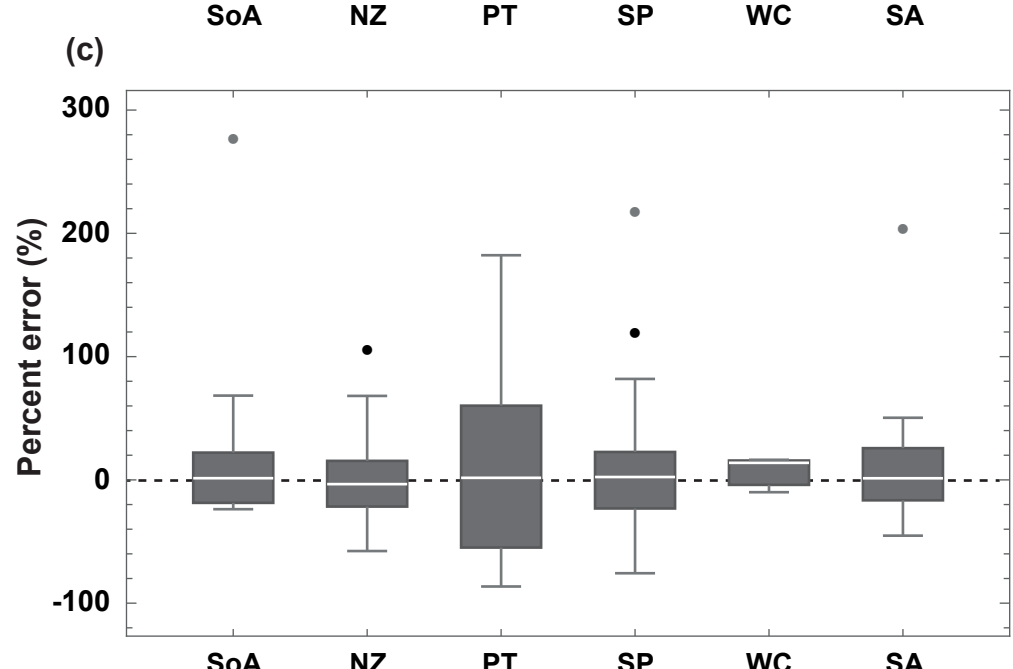
(c)
Percent error (%)
300
200
100
0
-100
SoA
NZ
PT
SP
WC
SA

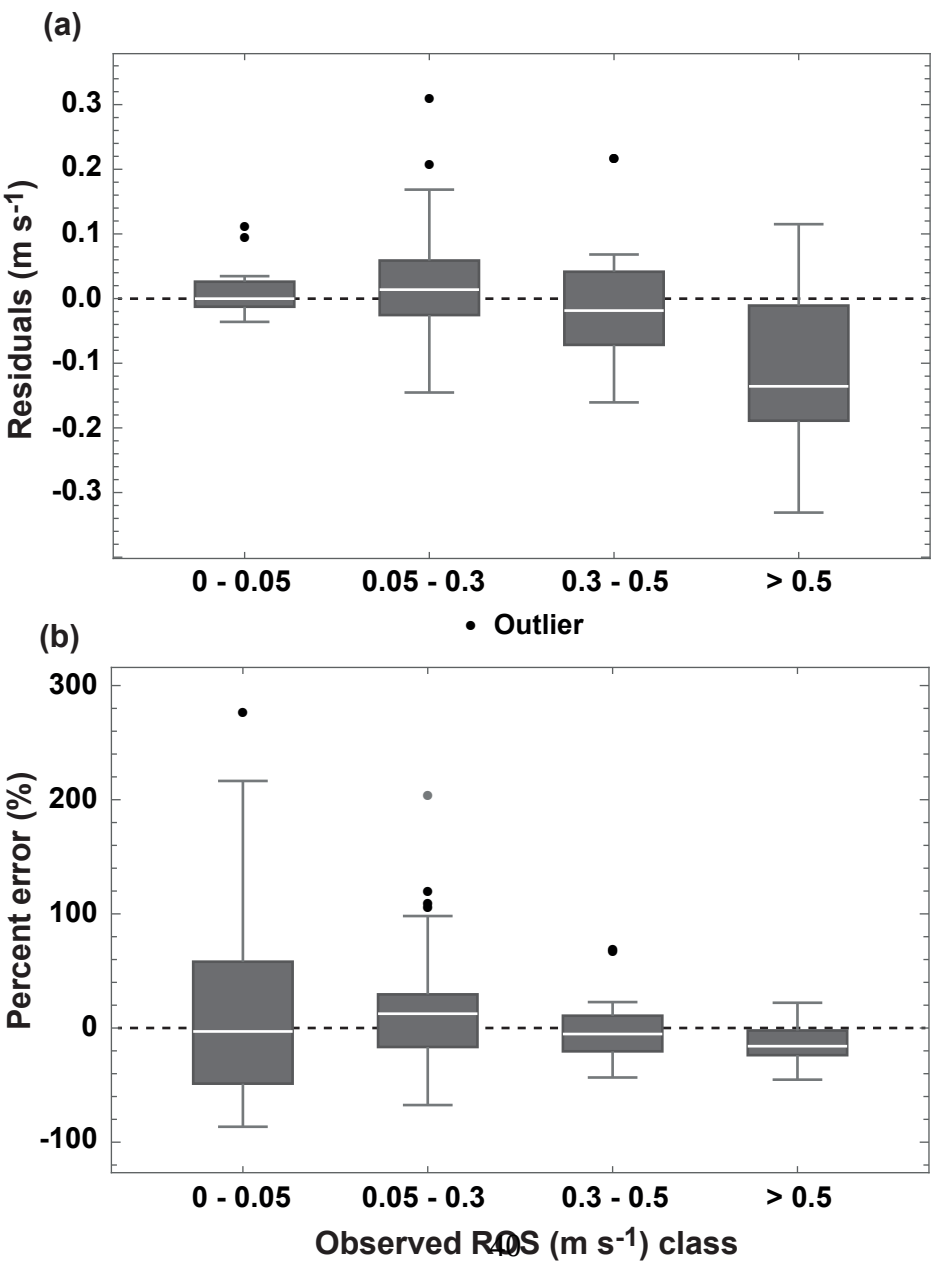
(a)
Residuals (m s-1)
0.3
0.2
0.1
0.0
-0.1
-0.2
-0.3
0 - 0.05
0.05 - 0.3
0.3 - 0.5
> 0.5
Outlier
(b)
Percent error (%)
300
200
100
0
-100
0 - 0.05
0.05 - 0.3
0.3 - 0.5
> 0.5
Observed ROS (m s-1) class

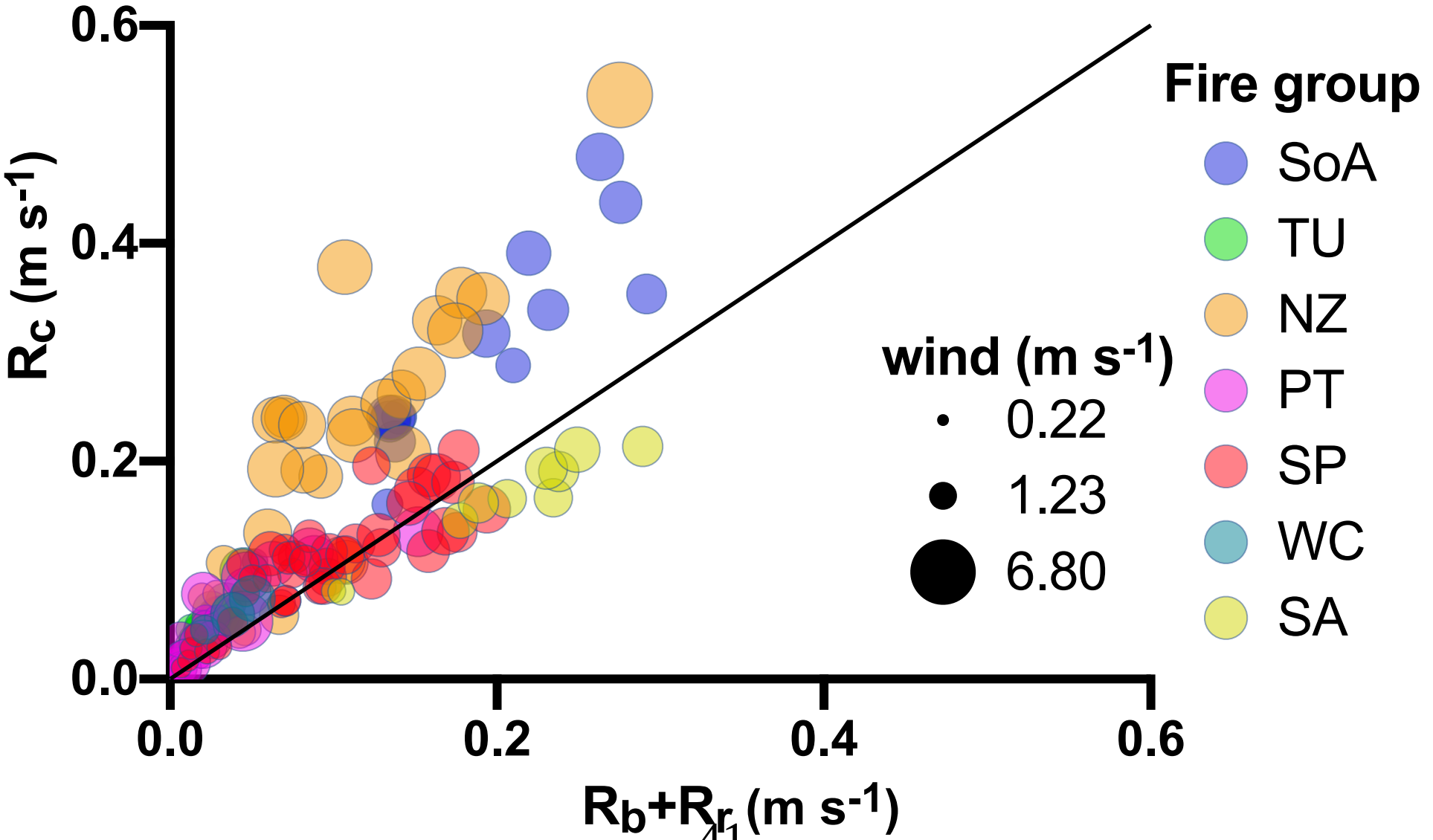
0.6
0.4
0.2
0.0
R_c (m s^{-1})
0.0
0.2
0.4
0.6
R_b+R_r (m s^{-1})
Fire group
SoA
TU
NZ
PT
SP
WC
SA
wind (m s^{-1})
0.22
1.23
6.80

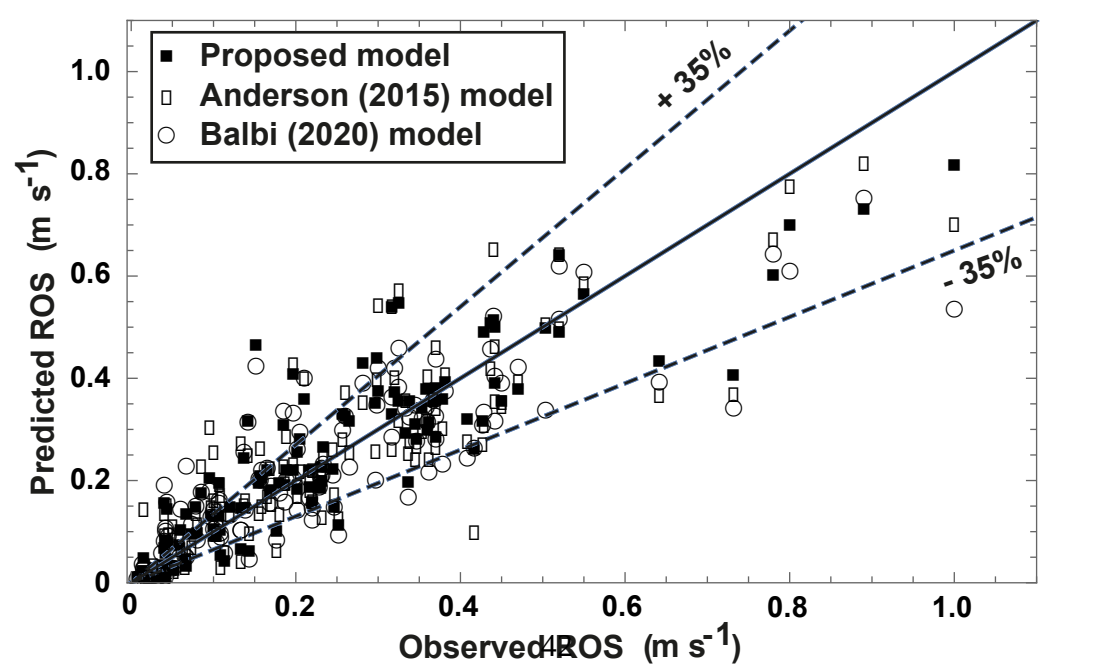
Proposed model
Anderson (2015) model
Balbi (2020) model
+ 35%
- 35%
Predicted ROS (m s-1)
Observed ROS (m s-1)
0
0.2
0.4
0.6
0.8
1.0

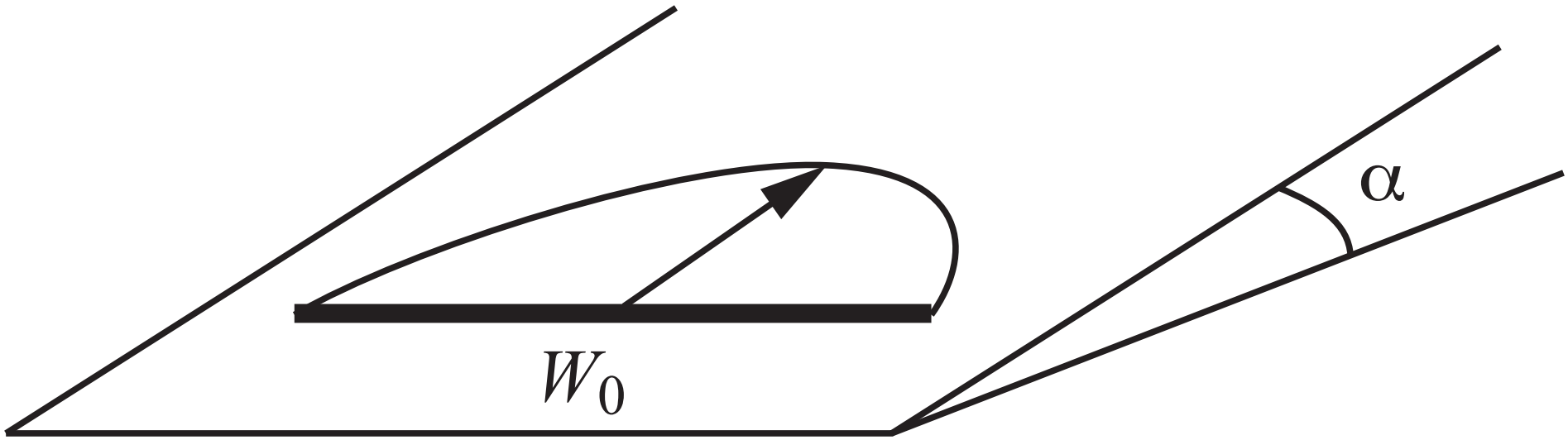

b)

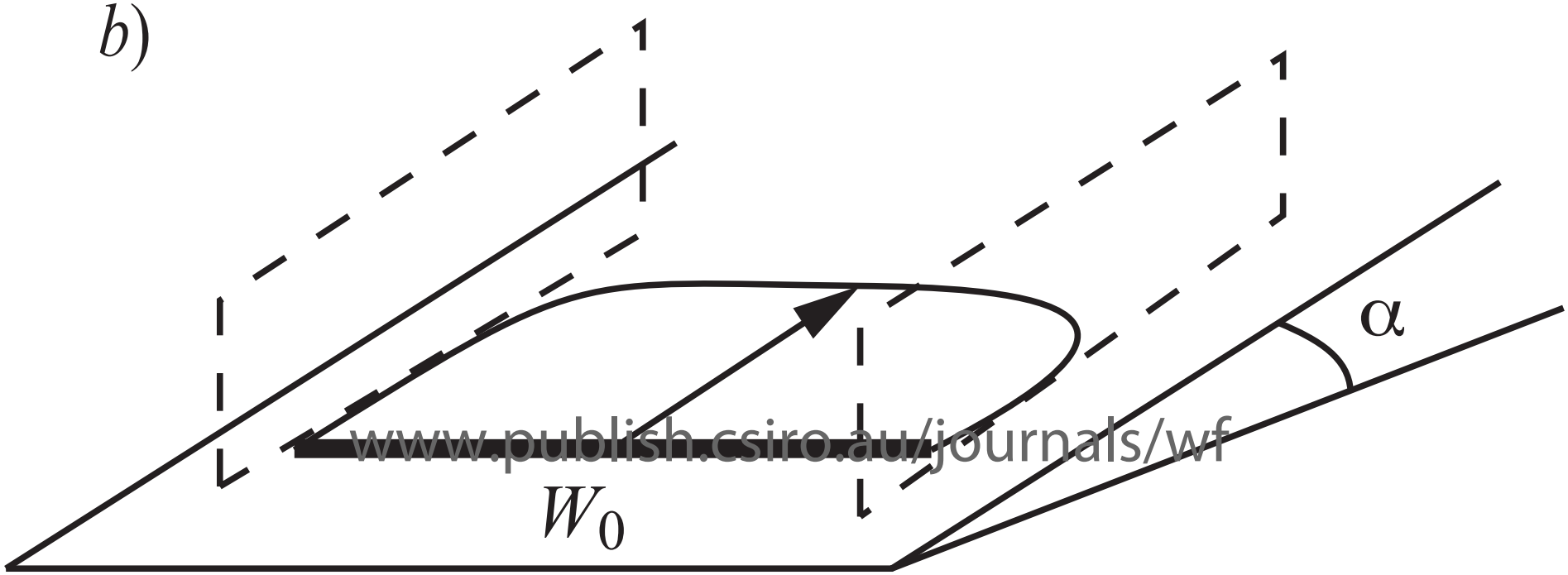

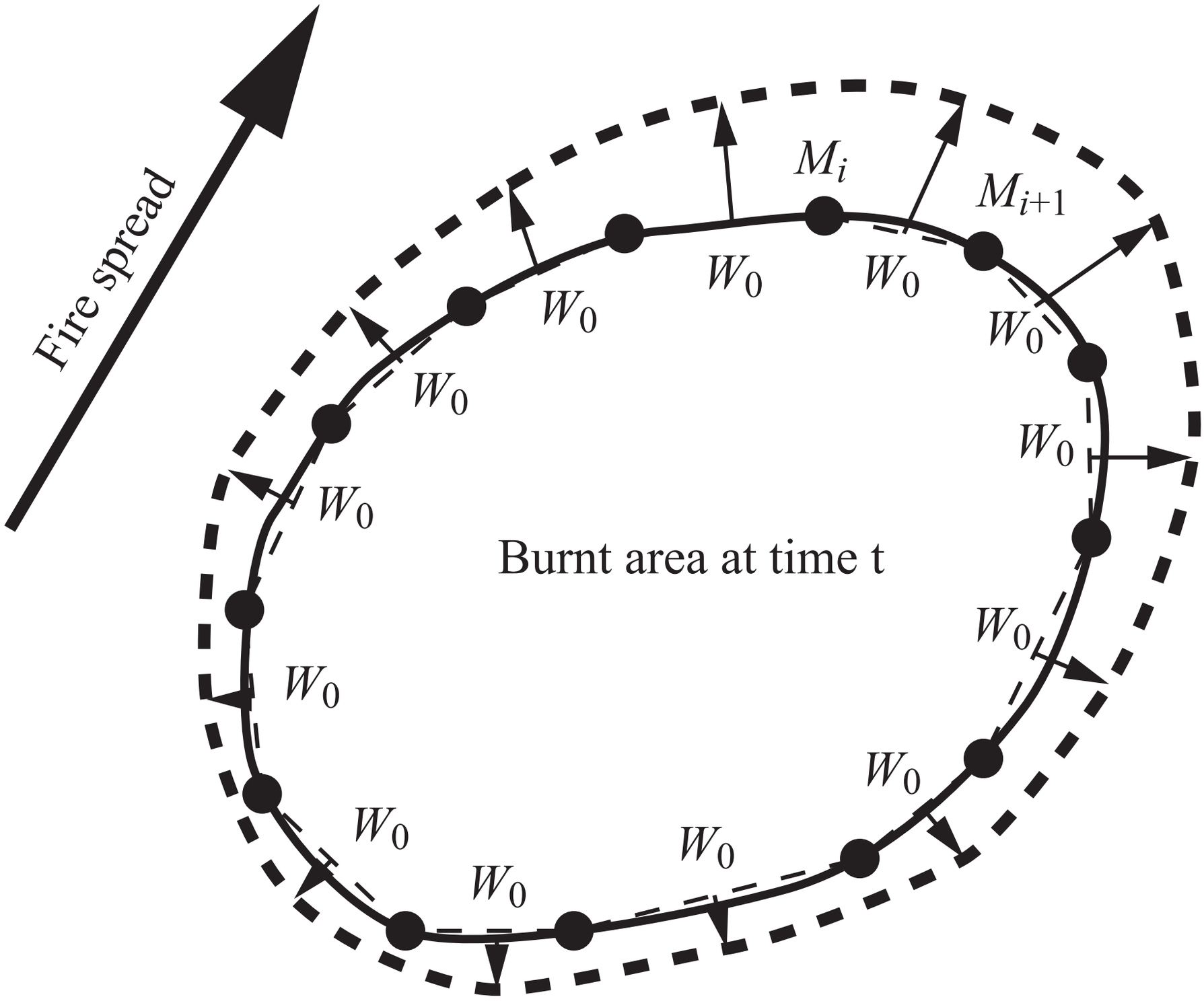
Fire spread
M_i
M_{i+1}
W_0
Burnt area at time t
Points M_i of the fire contour
Fire contour at time t
Fire contour at time t+Δt

Latin symbols

A	Radiant coefficient	
a	Scaling factor	
a_{lat}, a_{liv}, a_{up}	Intermediate Scaling factors	
a_M	Fitted model parameter	= 0.025
B	Stefan-Boltzmann constant (W m^{-2} K^{-4})	= 5.6 × 10^{-8}
C_{pw}	Specific heat of water (J kg^{-1} K^{-1})	= 4180
C_p	Specific heat of fuel (J kg^{-1} K^{-1})	
C_{pa}	Specific heat of air (J kg^{-1} K^{-1})	= 1150
g	Gravity acceleration (m s^{-2})	= 9.81
h	Fuel bed depth (m)	
H	Flame height (m)	
K	Law for drag forces	
K_1	Drag coefficient (s m^{-1})	= 130
L	Flame depth (m)	
l	Flame length (m)	
m	Fuel moisture content	
q	Ignition energy (J kg^{-1})	
r_{00}	Model coefficient	= 2.5 10^{-5}
R	Rate of fire spread (m s^{-1})	
R_b	Contribution of radiation of burning fuel bed to the ROS (m s^{-1})	
R_c	Contribution of convection to the ROS (m s^{-1})	
R_r	Contribution of flame radiation to the ROS (m s^{-1})	
s	Surface area to volume ratio of fuel (m^{-1})	
S	Leaf area by square meter (m^2 m^{-2})	
s_t	Air-pyrolysis gases mass ratio in the flame body	= 17
T	Mean flame temperature (K)	
T_a	Ambient temperature (K)	= 300
T_i	Ignition temperature (K)	= 600
T_{vap}	Vaporization temperature (K)	= 373
U	Sum of normal component (to the fire front) of the natural wind velocity and fire generated inflow coming from the burnt area (m s^{-1})	
$U(x)$	Air stream velocity within the burning fuel bed (m s^{-1})	
u_c	Upward gas velocity at the top of the flame base (m s^{-1})	
u_0	Upward gas velocity at mid-height flame body on flat terrain (m s^{-1})	
W_0	Ignition line width (m)	

Greek symbols

α	Terrain slope angle (°)	
β	Packing ratio	
δ	Extinction depth	
γ	Flame tilt angle (°)	
γ_c	Angle defined in fig. 1 (°)	
ε	Flame emissivity	
χ	Radiative fraction	
χ_0	Radiant factor	= 0.3
ΔH	Heat of combustion of the pyrolysis gases (J kg^{-1})	= 1.74 × 10^7
Δh	Heat of latent evaporation (J kg^{-1})	= 3 × 10^6
ρ_v	Fuel particle density (kg m^{-3})	
$\dot{\sigma}$	Derivative of the dead fuel load over time	

σ	Dead fine fuel load (kg m^{-2})	
ϕ	Heat flux per unit length (W m^{-1})	
τ_0	Flame residence time parameter (s m^{-1})	= 75591
τ	Flame residence time (s)	

Subscripts	
a	Related to air
b	Related to the flame base
c	Related to the convective warming
r	Related to the flame body
t	Related to total fuel (dead and live fuel)
w	Related to the fuel water

Acronyms	
CFD	Computational fluid dynamics
FB	Fractional bias
FMC	Fuel moisture content
LAI	Leaf area index
NMSE	Normalized mean square error
ROS	Rate of spread

Parameter	Default value	Effect on ROS	
		(+10%)	(-10%)
Surface area to volume ratio (m^{-1})	6000	+8.9%	**-10.4%**
Fuel density (kg m^{-3})	500	**-12.2%**	**+13.6%**
Heat of combustion of pyrolysis gases (J kg^{-1})	1.74×10^7	**10.8%**	**-10.2%**
Fuel specific heat (J kg^{-1} K^{-1})	2000	-8.4%	+9.8%
Fuel height (m)	0.5	+4.9%	-5.1%
Dead fuel moisture content	0.1	-4.4%	+4.7%
Dead fuel loading (kg m^2)	0.3	+0.8%	-1.5%
Total fuel loading (kg m^2)	0.5	-3.5%	+2.7%

Dataset [nb of fires]	NMSE [FB]			
	Proposed model	**Anderson *et al* (2015) model**	**Balbi *et al* (2010) radiative model**	**Balbi *et al* (2020) model**
New Zealand (NZ) [28]	0.111 [-0.02]	0.190 [-0.09]	30.956 [-1.77]	0.188 [-0.15]
Portugal (PT) [24]	0.308 [-0.14]	0.792 [0.04]	12.803 [-1.63]	0.418 [0.05]
Spain (SP) [44]	0.095 [-0.04]	0.095 [-0.16]	9.833 [-1.54]	0.146 [-0.03]
Australia (WC) [3]	0.018 [0.06]	0.146 [0.34]	48.232 [-1.92]	0.093 [0.00]
Australia (SA) [10]	0.213 [0.06]	0.241 [-0.08]	1.796 [-0.88]	0.261 [-0.04]
South Africa (SoA) [14]	0.048 [0.09]	0.056 [0.2]	9.735 [-1.53]	0.058 [0.16]
All [123]	0.132 [-0.03]	0.180 [-0.05]	11.528 [-1.56]	0.183 [-0.02]

Appendix A – Models for comparison purpose

Balbi et al. (2010) model

The first version of the Balbi model was presented in 2007. This simplified semi-physical model (Balbi *et al.* 2007) was designed to be used in operational situations. Following Albini (1985, 1986), this model assumed that radiation was the main heat transfer mode. But several limitations appeared: (1) some physical characteristics of the fire front were defined thanks to empirical relationships (for instance, the flame height is obtained with the McCaffrey correlation (McCaffrey 1979)); (2) many model parameters varied from a fire to another which lead to a non predictive model. Balbi *et al.* (2009) suggested the replacement of empirical relationships by physical laws. Actually, the flame height expression was derived from the equation for the vertical momentum applied to the flame and replaced the McCaffrey correlation. Balbi *et al.* (2010) came up with a better modelling for the radiative fraction and introduced a fresh cooling which models the backfire better. This improved radiative model was successfully applied to a set of laboratory experiments performed by Viegas (2004), under strong wind velocities (up to 11 m s^{-1}) with non-parallel wind and slope conditions. Moreover Weise *et al.* (2016) showed that the results given by this radiative model applied to laboratory experiments across litter fuel beds provided good results. But some shortcomings remained: (1) the model was still restricted to radiation heat transfer and then poorly represented a fire spread in well-ordered, vertically oriented fuel beds where convection is the dominant heat transfer mechanism (Wolff *et al.* 1991; Finney *et al.* 2013) and (2) the model still had empirical parameters and thus was not a predictive one. Later this last point was corrected and led to the radiative Balbi model defined by Eqn A1.

$$R = \min\left(\frac{S_t}{\pi},1\right)\left(\frac{S}{S_t}\right)^2 \frac{BT^4}{\beta\rho_v q} + AR\frac{(1+\sin\gamma-\cos\gamma)}{1+\frac{R\cos\gamma}{sr_{00}}} \quad \text{(A1)}$$

This model is fully predictive and a good agreement is obtained when it is compared to laboratory experiments in which radiation is the heat dominant transfer mechanism. Note that Eqn A1 is a two order polynomial equation and its solution is given by:

$$R = \frac{-(r_0 - R_b\cos\gamma - r_0 A(1+\sin\gamma-\cos\gamma)) + \left((r_0 - R_b\cos\gamma - r_0 A(1+\sin\gamma-\cos\gamma))^2 + 4r_0R_b\cos\gamma\right)^{\frac{1}{2}}}{2\cos\gamma} \quad \text{(A2)}$$

Anderson et al. (2015) shrubland model

Anderson *et al.* (2015) developed two generic-empirical models based on an extended dataset of shrubland fires. In the comparative model analysis used here we used the fuel height model (in the present notations and units):

$$R = \frac{1}{60} 5.6715\,(3.6\,U)^{0.9102}\,h^{0.2227}\,exp(-7.662\,m) \quad \text{(A3)}$$

With U being wind speed (m s^{-1} in the equation above) measured at 10-m in the open, h being fuel height (m) and m the moisture content of dead fine fuels. A correction is done for fires spreading in zero-wind conditions in order to avoid zero-ROS. This model is designed for fires with a fireline width (W_0) greater than 50 m. Otherwise, Anderson and her co-authors adapted Eqn A3 in order to take into account fireline width in the following way:

$$R = \left(\frac{1}{60} 5.6715\,(3.6\,U)^{0.9102}\,h^{0.2227}\,exp(-7.662\,m)\right)\frac{1}{1+9\,Exp(-0.00316\,W_0^2)} \quad \text{(A4)}$$

Balbi et al. (2020) model

Balbi *et al.* (2020) combined the modelling approach of Chatelon *et al*. (2017) that incorporate convective heat transfer with its radiative only model (Eqn A1) (Balbi et al. 2010) in order to obtain a complete simplified physical model that explicitly take into account convective and radiative heat transfer. The main equation of the model is written as follows (see (Balbi *et al.* 2020) for details):

$$R = \min\left(\frac{S}{\pi},1\right)\frac{BT^4}{\beta\ \rho_v\ q} + \frac{\mathrm{s}\ \Delta H}{q\ \tau_0}\min\left(h,\frac{2\pi}{s\ \beta}\right)\left(\frac{h}{2h+H}\tan\alpha + \frac{U\ Exp(-K_1\ \beta^{\frac{1}{2}}\ R)}{u_0}\right) + AR\frac{1+\sin\gamma-\cos\gamma}{1+\frac{R\cos\gamma}{s\ r_{00}}} \quad \text{(A5)}$$

Appendix B – Fire ignition line length

The improved model is a steady-state simplified physical model which gives the ROS for the most advanced point of the head fire front as shown in Fig. 8. The fuel bed width is usually small at laboratory scale (more or less 1 m) and the heat loss on the lateral edges of the fuel bed may be important and may play a role on the fire spread. But if the experimental apparatus is equipped with lateral walls, there is no lateral heat loss. As the (Catchpole *et al.* 1998) laboratory experiments were carried out across fuel beds lined with lateral walls, the model proposed by Balbi *et al.* (2020) does not take into account this lateral heat loss effect and the factor a_{lat} (Eqn 12) does not explicitly appear in the model because it is always equal to 1.

At field scale, except for trench fires, this effect may influence the head fire rate of spread only if the fireline width W_0 is smaller than a certain value. It is assumed that this effect does not play any role on the R if W_0 is greater than 50 m, which leads to the expression of the factor a_{lat} (Eqn 12).

The improved model is designed to be used under field operational conditions. For instance, if the model is inserted into a simulator, it does not need any mesh to calculate the fire contour. Each point of the fire perimeter at time $t+\Delta t$ is obtained with the external unit normal vector to the fire front from the fire perimeter at time t. As presented in Fig. 11, W_0 represents the distance between two consecutive points of the fire perimeter at time t. Indeed, as showed in Fig. 9, two points (M_i, M_{i+1}) of the fire contour at time t allow the calculation of a point of the new fire contour at time $t+\Delta t$ and W_0 which is the distance between M_i and M_{i+1}, acts as a new ignition line length. This is one major advantage of the model.

Appendix C – Expression of the convective heat flux

The convective heat flux is defined by Eqn 15. Combining Eqns 15, 16 and 18-19 yields

$$\phi_c = \frac{\Delta H}{2\tau_0}\sigma s \min(h,\delta)\left(\tan\alpha + U\frac{h}{h+\frac{H}{2}}\frac{Exp\left(-\frac{\beta_t}{\min\left(\frac{W_0}{50},1\right)}R\right)}{u_c}\right) \quad \text{(C1)}$$

The expression of upward gas velocity u_c computed at the top of the flame base does not change from (Balbi *et al.* 2020):

$$u_c = \frac{h}{h+\frac{H}{2}}\frac{u_0}{2} \quad \text{(C2)}$$

Substituting Eqn C2 in Eqn C1, yields:

$$\phi_c = \frac{\Delta H}{\tau_0 u_0}\sigma s \min(h,\delta)\left(\frac{u_0\tan\alpha}{2} + U\,Exp\left(-\frac{\beta_t}{\min\left(\frac{W_0}{50},1\right)}R\right)\right) \quad \text{(C3)}$$

Upward gas velocity at flame mid-height u_0 is also slightly changed because of the living part of the fuel. Indeed, following (Balbi *et al.* 2009), the simplified mass balance at flame mid-height equilibrate the rate of gas flow which enters the flame and the sum of the pyrolysis gases flow rate and the flow rate of the fresh air absorbed by the flame:

$$\rho u_0 \frac{L}{2} = (s_t + 1) L \dot{\sigma}_u \frac{h_u}{h} \quad \text{(C4)}$$

where ρ, s_t, h_u and $\dot{\sigma}_u$ are the gas density, a stoichiometric coefficient, the fuel bed depth under combustion and the derivative of the effective fuel load over time. The modelling of the ratio h_u/h is the same as in (Balbi *et al.* 2020), except for the leaf area changed in the total leaf area:

$$\frac{h_u}{h} = \min\left(1,\frac{h}{\delta}\right) = \min\left(1,\frac{2\pi}{S_t}\right) \quad \text{(C5)}$$

Finally, following exactly the calculations performed in Appendix B of (Balbi *et al.* 2020), the slight variation of the upward gas velocity is obtained:

$$u_0 = 2\frac{(s_t+1)}{\tau_0}\frac{\rho_v}{\rho_a}\frac{T}{T_a}\min\left(S,\frac{2\pi S}{S_t}\right) \quad \text{(C6)}$$

Moreover, using the definition of the leaf area $S = s\ h\ \beta$ and extinction depth $\delta = 2\pi/(s\ \beta_t)$ the following simplification is obtained:

$$\min\left(S,\frac{2\pi S}{S_t}\right) = \min\left(s\ h\ \beta,\frac{2\pi\beta}{\beta_t}\right) = s\ \beta\min\left(h,\frac{2\pi}{s\ \beta_t}\right) = s\ \beta\min\left(h,\delta\right) \quad \text{(C7)}$$

Substituting Eqns C6 and C7 in Eqn C3 yields:

$$\phi_c = \frac{\Delta H\rho_a T_a}{2(s_t+1)\rho_v T\beta}\sigma\left(\frac{(s_t+1)}{\tau_0}\frac{\rho_v}{\rho_a}\frac{T}{T_a}\min\left(S,\frac{2\pi S}{S_t}\right)\tan\alpha + U\ Exp\left(-\frac{\beta_t}{\min\left(\frac{W_0}{50},1\right)}R\right)\right) \quad \text{(C8)}$$

Finally, the contribution of the convective effects to the ROS is obtained in combining Eqns 3, 14 and C8:

$$R_c = a_M\min\left(\frac{W_0}{50},1\right)\frac{\Delta H\rho_a T_a\, s\sqrt{h}}{2q(s_t+1)\rho_v T}\left(\frac{(s_t+1)}{\tau_0}\frac{\rho_v}{\rho_a}\frac{T}{T_a}\min\left(S,\frac{2\pi S}{S_t}\right)\tan\alpha + U\ Exp\left(-\frac{\beta_t}{\min\left(\frac{W_0}{50},1\right)}R\right)\right) \quad \text{(C9)}$$